UNCLASSIFIED

SECURITY CLASSIFICATION OF THIS PAGE (When Data Entered)

DTIC FILE COPY

(1)

REPORT DOCUMENTATION PAGE

READ INSTRUCTIONS BEFORE COMPLETING FORM

1. REPORT NUMBER: AFIT/CI/NR 88-90	2. GOVT ACCESSION NO.
3. RECIPIENT'S CATALOG NUMBER	
4. TITLE (and Subtitle): AN EXAMINATION OF A SIMULATED MICROBURST FLOW AS SENSED BY A SINGLE DOPPLER RADAR	5. TYPE OF REPORT & PERIOD COVERED: MS THESIS
	6. PERFORMING ORG. REPORT NUMBER
7. AUTHOR(s): ELEANOR LEE SMITH	8. CONTRACT OR GRANT NUMBER(s)
PERFORMING ORGANIZATION NAME AND ADDRESS: AFIT STUDENT AT: UNIVERSITY OF MARYLAND	10. PROGRAM ELEMENT, PROJECT, TASK AREA & WORK UNIT NUMBERS
CONTROLLING OFFICE NAME AND ADDRESS	12. REPORT DATE: 1988
	13. NUMBER OF PAGES: 95
MONITORING AGENCY NAME & ADDRESS (if different from Controlling Office): AFIT/NR, Wright-Patterson AFB OH 45433-6583	15. SECURITY CLASS. (of this report): UNCLASSIFIED
	15a. DECLASSIFICATION/DOWNGRADING SCHEDULE

AD-A196 381

DISTRIBUTION STATEMENT (of this Report)

DISTRIBUTED UNLIMITED: APPROVED FOR PUBLIC RELEASE

17. DISTRIBUTION STATEMENT (of the abstract entered in Block 20, if different from Report)

SAME AS REPORT

18. SUPPLEMENTARY NOTES

Approved for Public Release: IAW AFR 190-1
LYNN E. WOLAVER Lynn Wolaver 14 July 88
Dean for Research and Professional Development
Air Force Institute of Technology
Wright-Patterson AFB OH 45433-6583

19. KEY WORDS (Continue on reverse side if necessary and identify by block number)

20. ABSTRACT (Continue on reverse side if necessary and identify by block number)

ATTACHED

DD FORM 1 JAN 73 1473 EDITION OF 1 NOV 65 IS OBSOLETE

UNCLASSIFIED

SECURITY CLASSIFICATION OF THIS PAGE (When Data Entered)

ABSTRACT

Title of Thesis: An Examination of a Simulated Microburst Flow as Sensed by a Single Doppler Radar

Eleanor Lee Smith, Master of Science, 1988

Thesis directed by: Dr. George J. Huffman
Assistant Professor
Department of Meteorology

The range and azimuthal limitations of a single Doppler radar in accurately determining velocity-based microburst parameters were studied. A vortex ring model was developed to simulate the microburst flow. The simulated velocities were vertically averaged over the lowest 500 meters of the flow using a Gaussian-squared weighting distribution. Smoothed values of radial shear parameters were examined for microbursts centered less than 30 km from a single Doppler radar; smoothing effects were minimal for azimuths of less than five degrees. Unsmoothed radial shear parameters were also compared as a function of azimuth, range, and arc length for microbursts centered from 15 km to 150 km from a Doppler radar. Detected radial shear decreases with increasing range and azimuth due to beam spreading. For a one-degree beam, the planned NEXRAD sampling rate, the difference in radial shear for a maximum 0.5-degree offset between 15-km and 150-km microbursts is 18%, creating non-existent fluctuations. For short arc lengths, the differences in radial shear parameters are small; they increase for

longer arc lengths but the shear magnitudes are small. Since microburst information has its structure in the radial direction, range alone has no significant effect on velocity-based microburst parameters detected by Doppler radars. At non-zero azimuths, increasing range has a strong effect due to beam spreading. But over one degree, the effects are small. Information gathered from the beam's outer edges will induce parameter error which increases with range, but this should be correctable in the NEXRAD software.

AN EXAMINATION OF A SIMULATED MICROBURST FLOW AS SENSED BY A SINGLE DOPPLER RADAR

by

Eleanor Lee Smith

Thesis submitted to the Faculty of the Graduate School of the University of Maryland in partial fulfillment of the requirements for the degree of Master of Science

1988

Advisory Committee:

Professor Anandu D. Vernekar
Associate Professor Robert G. Ellingson
Assistant Professor George J. Huffman

I wish to express my thanks to some of the many people who have helped me complete this project:

- Dr. George J. Huffman, my advisor, for his time, insights, and willingness to help me over my many hurdles.

- My other faculty committee members (Dr. Anandu Vernekar and Dr. Robert G. Ellingson) for their thoughtful and careful review of this thesis.

- My husband, Glenn, whose love and encouragement kept me going during some really stressful times.

- To Jeff Straight, whose talented artwork appears in Figure 1 of this thesis.

- My family, friends, co-workers, and Christian brothers and sisters for their help, prayers and "How's your thesis coming?" questions.

These people were an encouragement and motivational for me as I worked a full-time job, underwent major surgery, spent six weeks in a cast, travelled for my job, and still worked on this project.

"Where were you when I laid the earth's foundation?
Have you ever given orders to the morning
or shown the dawn its place?
Have you entered the storehouses of the snow
or seen the storehouses of the hail?
What is the way to the place
where the lightning is dispersed,
or the place where the east winds
are scattered over the earth?
Do you send the lightning bolts on their way?
Do they report to you, "Here we are" ?"

Job 38: 4, 12, 22, 24, 35

TABLE OF CONTENTS

LIST OF FIGURES

LIST OF TABLES

1. INTRODUCTION

On 24 June 1975, Eastern Airlines Flight 66 (EA 66) hit the runway approach lights while attempting to land at John F. Kennedy International Airport in New York City. Of the 124 persons on board, 112 were killed and the other 12 were injured. Only minutes before the crash, another Eastern flight nearly met a similar fate but was able to abandon its approach in time to avoid an accident. Both aircraft encountered a very strong wind shear. Other aircraft landing minutes before these two aircraft reported moderate to heavy rain, strong downflows and/or crosswinds, and loss of airspeed. The crash of EA 66 and other aircraft accidents sparked an interest in researchers to study these strong, unusual, and life-threatening wind shears.

1.1 A Look at Downbursts

Much of the pioneering study of these phenomena, as described below, was done by Fujita (1976). During an earlier study of the damage done by a "superoutbreak" of tornadoes, he noted a strange pattern in the damage done to an area of trees. From the air, the pattern resembled a starburst, with the trees blown outward from the center of the starburst. The damage pattern suggested that an intense downdraft had occurred, impacting the ground at the center of the starburst. His findings during the

investigation of the EA 66 crash suggested the presence of a similar downdraft. His first significant finding was the limited extent of the downdraft winds, occurring on a scale much smaller than the mesoscale. His second significant finding was the low altitude at which these winds occurred and their resemblance to a near-ground jet of wind. He established that such events routinely caused damage in a starburst pattern. Based on these findings, Fujita developed the concept of a "downburst". He defined a downburst as a strong downrush of air (Fig. 1) which diverges in all directions near or at the ground. He then subdivided downbursts into "macrobursts" and "microbursts" dependent upon whether the downburst diameter was larger or smaller than 4 km. Although his theories initally met some resistance, since about 1980 there has been a great deal of research done into the physical processes responsible for microbursts, the different types of microbursts, and, most importantly to the operational aviation forecaster, methods for detecting and forecasting microbursts.

Fujita (1985) defined microbursts as downbursts with damaging winds extending outward in a starburst pattern, having a horizontal extent of 4 km or less, with a speed differential of at least 10 m/s between the maximum wind speeds on opposite sides of the downburst. Individual microbursts usually last less than 10 minutes and are at

peak intensity for 2-4 minutes (McCarthy and Wilson, 1985). However, multiple microbursts and microburst lines or "families" can extend a microburst event to over an hour (McCarthy, Wilson, and Hjelmfelt, 1986). Even though the affected area is small, an intense microburst could cause damaging winds as high as 75 m/s (Fujita, 1985). Microbursts usually intensify upon impact with the ground, averaging a speed differential of about 12.5 m/s upon initial impact but doubling to about 25 m/s after only a few minutes (McCarthy and Wilson, 1985). The microburst boundary propagates outward more slowly than the speed of the winds inside the microburst. The slower outward propagation results from the pressure gradient that is formed between the environment and the outrushing air from the microburst. A strong enough gradient forces the air to curve upward and back, resulting in the formation of a horizontal vortex ring around the center of the downflow (Figs. 1 and 2). The winds below this vortex ring are continuously accelerated as the ring stretches and expands (Fig. 3). Results of the Northern Illinois Meteorological Research on Downbursts (NIMROD) and Joint Airport Weather Studies (JAWS) Projects indicate that most vortex rings are first observed between 1-2 km in distance from the center point of the microburst, that is, the point of divergence (Fujita, 1985).

The presence of a microburst is hard to determine from the standard meteorological variables, unlike a macroburst which is accompanied by a dome of high pressure, gusty winds, and abruptly cooler temperatures. Ambient and dew-point temperatures associated with microbursts can either be warmer or cooler than the environment (Fujita, 1985). This is thought to occur because the air may either warm as it descends dry-adiabatically to the surface or cool if there is sufficient evaporation to maintain a moist-adiabatic descent. Lower dew-point temperatures are thought to be caused by the entrainment of dry air into the microburst as it descends. Observing and monitoring the microburst wind field can be very difficult because of the small scale of the microburst. Because anemometers can only provide wind readings for a point, not an area, the wind field could be totally missed by standard airfield anemometer instrumentation (Fujita, 1985). Before the NIMROD and JAWS Projects, Fujita assumed heavy rain occurred with all microbursts. The results from these projects indicated otherwise; 36% of the NIMROD microbursts and 83% of the JAWS microbursts had no accompanying rain at the surface (Fujita, 1985). His statistics showed that raindrops in microbursts occurring in dry regions often evaporated completely before reaching the ground. Therefore, Fujita made a further distinction in his study of microbursts, dividing them into categories as either a "wet" microburst or a

"dry" microburst. Although both types of microbursts may have rainfall associated with them, the classification of the type of microburst that occurred depended upon the amount of rainfall reported at the surface.

Wet microbursts occur in storms with high radar reflectivities and high precipitation rates; in the humid regions of the United States, such as most of the South, almost all microbursts are accompanied by heavy rainfall (Fujita, 1985). According to a study of microbursts in the mid-South (Rinehart and Isaminger, 1986), air mass thunderstorms and squall lines account for the majority of the wet microbursts. A characteristic environment for a wet microburst is an atmosphere with an unsaturated, near-adiabatic boundary layer and deep mid-level moisture that allows for the growth of deep convection and heavy precipitation (Eilts, 1986). A shallow layer of drier air is also present in mid-levels (around 600 mb) which provides the evaporational cooling that sets off the downrush of air (Caracena and Maier, 1987). Rinehart and Isaminger (1986) showed that more than 85% of the microburst events they studied had radar reflectivity cores stronger than 50 dB and many had rainfall rates greater than 75 mm/hr. These strong reflectivity cores provide a way to track the development of the microburst on a conventional noncoherent radar since the sinking of the reflectivity core, as observed by the radar, is a good

precursor of a microburst. Other technologies, particularly those using Doppler principles, will show other important microburst precursors, such as rotation and convergence.

Dry microbursts occur with high-based cumulus clouds and are often preceeded by virga. These storms usually display low reflectivities and low precipitation rates. These inocuous conditions can deceive the forecaster and pilot alike into believing the atmosphere is fairly tranquil. A typical atmosphere for a dry microburst shows a deep dry-adiabatic subcloud layer and strong conditional instability aloft. The highly unstable lapse rate is thought to be the key in maintaining the downdraft's negative buoyancy against adiabatic warming until it reaches the surface (Elmore, 1986). Virga is often the only visual clue to the observer that the microburst is about to occur. Another possible visual clue may be the appearance of the horizontal vortex generated by the downflow (Fig. 2). It may become visible as the wind picks up dust, loose soil or sand, but this only confirms the event is already occurring, providing no lead time for the duty forecaster or the unsuspecting aviator.

Most conventional radars provide little help in detecting a dry microburst because of the low radar reflectivities associated with these downbursts. A study

done by Kessinger, et al.(1986), observed that the average reflectivity at 500 m for the 32 low-reflectivity microbursts studied during the JAWS project was 21 dBZ, with actual values ranging from 5 to 30 dBZ. They noted that the lack of correlation between reflectivity and strength of the microburst was similar to earlier results by McCarthy, et al. (1983).

Conventional radars are better at detecting the high reflectivity cores associated with wet microbursts. Studies of wet microbursts by Caracena and Maier (1987) and Burrows and Osborne (1986) showed these microbursts were embedded in heavy rain with reflectivities of 40-50 dBZ. A study of high-reflectivity storms by Roberts and Wilson (1986) showed tremendous growth in storm strength prior to the microburst occurrence, with reflectivities reaching as high as 60-65 dBZ. A reflectivity notch will sometimes be apparent as drier air is entrained into the cloud through convergence. The descent of the core of high reflectivity echoes is an important signal that the microburst is imminent (Roberts and Wilson, 1984). Careful monitoring of storm development can provide precious time to issue a microburst warning but the reflectivities alone can provide no clue to downdraft wind speeds; this requires additional information not available from conventional radars.

Fortunately, the installation of Doppler radars around the country is planned through the Terminal Doppler Weather Radar (TDWR) and Next Generation Weather Radar (NEXRAD) programs to upgrade both civilian and military airport facilities; these programs were decided upon at least partially because of the capability of a Doppler radar to detect the presence of a microburst and the need for a man-machine mix to provide the most effective warning service to aviators.

A variety of mechanisms are thought to cause these violent downdrafts. The summary by Roberts and Wilson (1984) includes precipitation drag, penetrative mixing within the cloud, evaporative cooling associated with dry air entrainment into the cloud, cooling by melting precipitation within the cloud, and rapid evaporation and/or melting of precipitation in a dry adiabatic layer below the cloud base. They concluded that the last mechanism dominated by more than a factor of two over the other main contributors, namely in-cloud precipitation melting and precipitation loading, in generating the dry microbursts which descend from shallow, high-based virga-producing cumulus. Caracena and Maier (1987) showed similar findings in their study of a wet microburst, although for a wet microburst they found that negative buoyancy was caused by evaporation into a dry mid-level layer. This factor exceeded precipitation loading

effects by an order of magnitude, although precipitation loading still enhances negative buoyancy in a wet microburst. Eilts (1986) also demonstrated that evaporative cooling below the cloud base was not significant for the events associated with heavy precipitation due to the more moist atmosphere through which the microburst was descending. The common denominator for all microbursts, then, seems to be evaporative cooling, whether in a shallow dry mid-level layer (wet microbursts) or in a dry subcloud layer (dry microbursts). The evaporative cooling lowers the temperature of the air within the cloud, or just below it, below the environmental temperature. This leads to violent downdrafts because the cooler air accelerates as it sinks adiabatically to the surface.

1.2 A Look at Radars

Radars send out pulses of electromagnetic energy that reflect off targets and return to the radar antenna. The amount of power returned to the radar provides information on the target's location and equivalent cross-section. The kind of target information a radar can distinguish depends upon the wavelength of the radar. A 1-cm wavelength radar can detect non-precipitating clouds (Battan, 1973) but its signal is quickly attenuated in a heavy rainshower. Conversely, a 10-cm radar can detect areas of rainshowers

very well, but the wavelength is too large to detect cloud droplets. The type of radar used, then, depends upon the type of phenomena one wishes to study or detect. Radar systems can also provide instantaneous information on storm motions when they are equipped to detect the Doppler shift in reflected signals.

The Doppler principle states that electromagnetic waves travelling from a target that is moving towards an observer will become bunched together, shortening the wavelength and increasing the frequency from the original values. Likewise, when a target is moving away from an observer, the frequency of the energy reflected off it is lower than the frequency of the original signal because the motion of the target lengthens the wavelength of energy returning to the observer, the radar. By measuring the shift in frequency between the transmitted and returned signals, Doppler radars are able to accurately measure the velocity of targets along the radar beam.

The targets any radar can accurately detect depend upon the wavelength and pulse repetition frequency of the given radar. The maximum range at which velocities can be accurately detected, specified by half the interval between pulses multiplied by the speed of light, is called the MAXIMUM UNAMBIGUOUS RANGE:

$$R(max) = c/(2\ PRF) \qquad (1)$$

where "c" is the speed of light and "PRF" is the pulse repetition frequency.

For a Doppler radar, the maximum radial velocity which can be measured is the MAXIMUM UNAMBIGUOUS VELOCITY, the speed at which a target moves half a wavelength between radar pulses, as given by:

$$V(max) = (\lambda)\ PRF/\ 4 \qquad (2)$$

where λ is the radar's wavelength.

A large PRF increases V(max) but decreases R(max). For a 5-cm radar to be capable of measuring velocities to 30 m/s, the higher end of average observed microburst velocities, a PRF of 2400 pulses per second (pps) is required. For these conditions, R(max) would be 62.5 km (or about 40 mi) which is not very useful operationally due to the likelihood of range folding. Range folding occurs when strong targets at ranges greater than R(max) reflect energy back to the radar. This energy doesn't arrive back at the radar until after the next pulse has already been transmitted. Since the radar determines the distance the signal has travelled based on the elapsed time since the most recent pulse, the targets to appear much closer to the radar than their actual distances. The energy returned from these targets would actually overlap the returns from targets within the maximum

unambiguous range, giving rise to the name "second trip echoes" which is used to describe these returns. To accurately view targets at larger ranges and the same PRF, a smaller maximum unambiguous velocity must be accepted, which can lead to velocity aliasing, a phenomenon which occurs for velocities that is analogous to range folding. Obviously, then, some kind of trade-off between wavelength and pulse repetition frequency must be made. Fig. 4 shows the trade-off between V(max) and R(max) for several different wavelengths.

A pulsed radar receives its returned signal in an echo volume one beamwidth in cross-section and a half a pulse length in length (Fig. 5). Within this volume are varying frequency shifts corresponding to the particles of various size, shape, speed, and composition which reflected this energy. The Doppler radar processes and separates the power in the various frequency shifts, resulting in the Doppler spectrum, the amount of power received by the radar for each frequency. Large drops usually return the maximum amount of power to the radar since the reflected power is proportional to the radius of the drop raised to the sixth power (r^6). These large drops tend to be less affected by small turbulent eddies, moving more with the mean flow, so their frequency shift, the maximum power in the frequency shift spectrum, can be used to determine the mean Doppler velocity within that

echoing volume. Even without the larger drops, the movement of smaller drops can provide important information. Knowledge of the movement of smaller particles or hydrometeors such as pollutants or salts in the atmosphere can often be used to detect wind shears, such as those associated with a dry microburst. The shape of the Doppler spectrum depends on the characteristics of the radar and the targets being interrogated. A volume containing small droplets and weak wind shear will have a sharp, narrow Doppler spectrum curve while one with large drops and strong shear will have a wider curve. In general, a wider spectrum corresponds to a more turbulent atmosphere (Fig. 6), while the most reliable Doppler estimates of mean motion within or near a target volume are obtained from spectra with narrow widths and sharp peaks (Covey, 1983). This kind of spectrum can be achieved even for a turbulent atmosphere by increasing the antenna size, slowing the rotation rate, or decreasing the R(max). Slowing the rotation rate increases the amount of time the radar samples each volume element. Increasing the size of the antenna or decreasing the R(max) decreases the size of the echo volume, which should decrease the amount of variability in particle motion (Covey, 1983). However, decreasing R(max) can result in range folding, as mentioned previously.

Three types of two-dimensional displays are available on a Doppler radar: equivalent reflectivity, as on a conventional (noncoherent) radar; radial "Doppler" velocity, measured by the difference in phase between the transmitted and returned pulses; and the Doppler spectrum, or the spectrum width. Graphical radial velocity displays usually use different colors for motions towards and away from the radar. By convention, velocities towards the radar are considered negative while velocities away from the radar are positive. The Doppler spectrum also uses a color display; the most vivid colors are usually associated with large spectral width and indicate the areas with the highest probability of turbulence and/or wind shear. These last two capabilities make Doppler radars a promising tool in the efforts to detect the presence of microbursts prior to their actual occurrence. Doppler weather radars usually have large antennas, providing high gain, decreased side lobe contamination and high resolution in azimuth. These characteristics allow detection of clear air motions and flow in areas without precipitation or cloud droplets. It is hoped that this clear air capability will greatly improve the efforts in detecting dry microbursts, which elude conventional radars.

1.3 Using Doppler Radars

Doppler radars have been an important part of microburst research in recent years. But Doppler radars, like any piece of manmade equipment can give only incomplete information. There are numerous sources for potential error. These include such things as smoothing, geometrical considerations, and ground clutter contamination. Such things as atmospheric refraction and the earth's curvature make it impossible to know the exact height of the beam above the Earth's surface. In addition, ground clutter can significantly contaminate the radar signal, especially close to the ground where the microburst diverges. The radar beam has a finite volume; the width of the beam partially determines the degree of smoothing of the wind field. If the wind field is smoothed too much, the velocity peaks are flattened. Velocity extremes are impossible to distinguish, the amount of shear cannot be measured, and a microburst could be totally missed.

Doppler radars can determine wind speeds at various levels by scanning the atmosphere in layers. By sampling using a specified azimuth angle, a polar grid is determined. After the radar has rotated the full 360 degrees, the antenna elevation angle increments and the whole process starts over again. This process is repeated

until the entire volume of interest has been sampled, usually about two to three minutes (Wilson, et al., 1984). This information can be processed to provide a look at wind flow and reflectivities. A common azimuthal beam is one degree, which yields a pulse volume of about 300 m in both the horizontal and the vertical (Wilson, et al., 1984). The NEXRAD radar will have a wavelength between 10 cm and 11 cm, three PRF options (the highest being 1300 pps) and a 1-degree beamwidth; it will take six minutes to scan nine levels (NEXRAD JSPO, 1986).

The NIMROD and JAWS projects each used three Doppler radars, in a triangle formation encompassing their area of interest, to try to account for some of these problems. With each of the radars viewing the same microburst, the position of the microburst and its wind speeds can be more accurately pinpointed. Operationally, however, using three Doppler radars is not financially feasible. So it is necessary to determine how to best use a single Doppler radar to detect severe weather.

An FAA study done by Wilson, et al. (1984) listed several general requirements for adequate detection of microburst winds. The radar must be able to measure reliable velocities in the lowest kilometer of the atmosphere without regard to any precipitation that is occurring. It should be able to observe the lowest 100 m

of the atmosphere, although they conceded that observing the lowest 100-500 m will usually provide a rough estimate of the velocity differential below 100 m. The radar must be within 40 km of the airport; for an elevation angle of 0 deg, the center of the beam would be about 100 m above the ground at this distance from the radar. Ground clutter could further reduce this to an effective beam height of 200-400 m. In order to see the lowest 100 m of the atmosphere, though, the radar would need to be within 15 km of the airport (Wilson, et al., 1984).

In addition, the operational usefulness of the radar is significantly influenced by the radar's position in relation to the area it's viewing, usually an airport runway. If the radar is to be used to determine the headwind-tailwind components along the different flight paths of the aircraft, then it needs to be centrally located at the airport. To know the winds precisely for one particular flight path, the radar would need to be located parallel along the line of that runway; it could then be located at an off-airport site. An off-airport site would also allow scanning of the atmosphere high above the airport for any incipient microbursts. But this makes direct measurements impossible for any other flight paths and runways at the same airport. To quantitatively measure the shear for at least some of the flight paths, an on-airport siting of the radar is best (Wilson, et al.,

1984). Because of the cost of these radars, though, the NEXRAD and TDWR project offices plan in some cases to make one radar serve more than one airfield. For example, in the Washington, D.C. area, installation of a Doppler radar is planned in Sterling, VA along the northwest boundary of Washington/Dulles International Airport (IAP) that will also provide information to Washington/National Airport, about 37 km (20 nmi) away, Andrews AFB D.C., 55.6 km (35 nmi) away, and Baltimore-Washington IAP, about 92 km (50 nmi) away (Leone and Scott,1984).

With these considerations, we need to know the capability of a finite radar in sensing microburst parameters, in particular the effect of the distance or size of a microburst on the accuracy and sensitivity of the radar. We would expect the radar to be accurate at close ranges due to the large number of beamwidths required in the azimuthal direction to sample the total microburst flow pattern. But with increasing distance, more and more of the total microburst flow is included in every beamwidth. The inherent smoothing this causes should decrease the radar's sensitivity and accuracy in measuring typical microburst parameters.

A similar study was done by Jendrowski (1986) of mesocyclone Doppler velocities sensed by a single Doppler radar. He simulated 3 basic mesocyclone circulations and

evaluated them using a single Doppler radar at different range and azimuthal sampling orientations. These different orientations were used to simulate real features of interest, which are almost never located directly in the center of the beam. By comparing the circulation parameters calculated for a particular azimuth angle to those calculated for an offset angle of 0.5 deg to either side of that angle for a 1-deg beamwidth radar, we can determine what error is induced in the information due to the offset. One case showed a 24% change in the magnitude of the tangential shear and a 27% change in angular momentum over adjacent range gates as the sampling orientation was varied. Jendrowski's results showed increasing sensitivity and variability for increasing range in the tangential shear, average and maximum rotational speed, and azimuthal diameter with angular orientation and sampling. Because microbursts are also small in size, with diameters of generally 4 km or less, the problem we chose to examine was: What changes are seen in downburst velocity-based parameters due to range and azimuthal orientation?

We simulated a microburst flow, determined the most important velocity parameters, and examined how these parameters differed from the analytic (simulated) value based on the range of the microburst from the radar and its azimuth angle. We also investigated the inherent

smoothing that occurs with range and how it affects the flow detected by the radar. Finally, we discuss our results and draw some conclusions based on them.

2. THE PROBLEM

In studying the range and azimuthal orientation dependence of microbursts, we made some assumptions which allowed us to examine changes based purely on range and azimuthal orientations; we assumed a circular and stationary microburst (i.e., axially symmetric and time-independent) and uniform beam-filling. To determine which parameters to calculate from the simulated microburst flow, we compiled a list of factors used in studies by Fujita (1985, 1986), Rinehart and Isaminger (1986), Elmore (1986), Roberts and Wilson (1984, 1986), and Eilts (1986). We also included parameters used by Hjelmfelt (1984), Wilk (1985), and Wilson, et al. (1984). This compilation showed the most frequently used parameters were velocity-based ones such as radial shear and/or parameters based on the radial shear such as the maximum radial shear and the normalized shear. Velocity-based parameters provide information on microburst winds that reflectivities cannot, and are much easier to model and evaluate quantitatively than the spectrum width, so we also chose to use velocity-based parameters for our study. We developed a model to analytically specify a microburst flow, chose parameters that appeared to be the most important in describing this flow, and then extracted those parameters for microbursts centered at different ranges from the radar.

2.1 Flow Simulation

We began with a model based on infinitesimal flow dipoles called a doublet sheet (Fig. 7a). The model is a three-dimensional circular axisymmetric doublet sheet of variable intensity, developed by Zhu and Etkin (1985) to generate a microburst velocity field near the ground for use in investigating the landing and take-off of airplanes under microburst conditions and to provide on-line real-time simulations for pilot use in flight simulators. The model was developed using research published by Fujita (1976) on the microbursts that claimed the lives of 112 people in the tragic EA 66 crash. Using Fujita's findings of the height of the cloud base at approximately 1 km above the ground and maximum wind speeds, based on the reconstructed wind profile, of about 11.6 m/s in the vertical and 18 m/s in the horizontal, they constructed a classic fluid-dynamic model with an incompressible, inviscid, irrotational flow. The model considers only the region of the atmosphere closest to the ground. Variable temperatures and hydrostatic effects, i.e. evaporative cooling, were not included in the model. To model the flow, Zhu and Etkin used a planar distribution of singularities at a height, H, above the ground. To insure the ground plane was a stream surface, they introduced an image singularity at z= -H as a mirror image doublet sheet of opposite sign to the singularity at z= +H. The size,

position, and strength of the singularities can be varied to study different cases.

The doublet sheet concept was modified by Dr. George Huffman to model microburst flow as a vortex ring, which allowed us to use solid body rotation, a physically reasonable scheme, to eliminate velocities which increased without bound in the center of the near-surface downburst rotor. This adaptation is reasonable in light of recent research by Ivan (1986), who also developed a mathematical vortex ring model of a microburst which resembles an idealized mature stage flow pattern as seen in the Joint Airport Weather Studies (JAWS) Project. Ivan's model is also a three-dimensional axisymmetric circular flow field; the radial and axial velocity components are calculated from the stream function for the flow field. In a reply to Ivan's work, Etkin (1987) states that Ivan's method is "exactly equivalent to that of the uniform doublet sheet." However, Zhu and Etkin's model was developed to model winds for take-offs and landings; they were not concerned about modelling the winds at the center of the microburst rotor.

As in the doublet sheet model, we introduced a below-ground image vortex ring to satisfy the boundary condition that the ground be a material surface, that is the flow would not pass through the ground. Contributions from

both above-ground and below-ground (mirror image) fields describe the microburst flow and are used to generate model output. Our vortex ring model (Fig. 7b) simulates a flow that is concentric about the z-axis, at a height z′ and radius, a, using a Cartesian frame of reference. Knowing the vortex circulation strength, w′, the vorticity vector ($\vec{w}'$) at each point around any of the rings can be written as:

$$\vec{w}' = -w' \sin\theta \, \hat{i} + w' \cos\theta \, \hat{j} \qquad (3)$$

where θ is the angle from $\vec{x}$ to $\vec{x}'$ (see Fig. 7b) in cylindrical coordinates. A vector potential, $\vec{B}(\vec{x})$, with a differential volume element dV at $\vec{x}'$ can be defined as:

$$\vec{B}(\vec{x}) = (1/4\pi) \int w'/S \; dV(x') \qquad (4)$$

where $S = [\Delta z^2 + a^2 + x^2 - 2 a x \cos\theta]^{1/2}$.
Isopleths of $\vec{B}(\vec{x})$ can be interpreted as a stream function for the rotational portion of the flow.

Substituting equation (3) into equation (4) around the ring, and with w′ equal to zero otherwise, the vector potential can be written as:

$$\vec{B}(\vec{x}) = w'/4\pi \int_0^{2\pi} (-\sin\theta \, \hat{i} + \cos\theta \, \hat{j})(a \, d\theta) / S \; (z, a, \theta) \qquad (5)$$

Since $(\sin\theta)/S$ is odd function of θ, we know that

$$-\sin(-\theta)/S(-\theta) = \sin(\theta)/S(\theta) \quad \text{and} \quad \int_0^{2\pi} \sin\theta / S \; d\theta = 0.$$

Since $(\cos\theta)/S$ is even function of θ, due to symmetry, we also know that

$$\int_0^{2\pi} \cos(\theta)/S \; d\theta = 2 \int_0^{\pi} \cos(\theta)/S \; d\theta .$$

Applying these relationships to equation (5), the vector potential can be written:

$$B(x) = aw'\hat{j}/2\pi \int_0^{\pi} \cos(\theta)\, d\theta / [\Delta z^2 + a^2 + r^2 - 2a\cos(\theta)]^{1/2} \quad (6)$$

where $S = [\Delta z^2 + a^2 + r^2 - 2 a r \cos\theta]^{1/2}$ and r is the distance from the center of the vortex ring to the position x in the plane of the vortex ring.

The rotational velocity is the curl of the potential:

$$\vec{u} = \vec{\nabla} \times \vec{B}$$

$$= \hat{z}\, w'a/2 \quad [r^{-1} \int_0^{\pi} (\cos\theta \, d\theta)/S - r \int_0^{\pi} (\cos\theta \, d\theta)/S^3 +$$

$$a \int_0^{\pi} (\cos^2\theta \; d\theta)/S^3] + \hat{r}\, w'a\, \Delta z/2\pi \int_0^{\pi} (\cos\theta \; d\theta)/S^3. \quad (7)$$

We also know that the velocity is non-divergent:

$$\vec{\nabla} \cdot \vec{u} = w'a/2 \quad [\, r^{-1} \int_0^{\pi} ((-1/2)\ 2\ \Delta z\ \cos\theta\ d\theta)/S^3 -$$

$$r \int_0^{\pi} ((-3/2)\ 2\ \Delta z\ \cos\theta\ d\theta)/S^5 +$$

$$a \int_0^{\pi} ((-3/2)\ 2\ \Delta z\ \cos^2\theta\ d\theta/S^5) + \Delta z/r \int_0^{\pi} (\cos\theta\ d\theta)/S^3 +$$

$$\Delta z \int_0^{\pi} (-3/2)(2r-2a\cos\theta)\cos\theta\ d\theta/S^5 = 0. \qquad (8)$$

The basic vortex ring program was developed from these equations by Dr. George Huffman. The program was expanded to allow a total of four coaxial vortex rings. The number of vortex rings, the vortex circulation strength, the ring radius and the ring altitude were variables to be specified by the user and input when prompted in the program. Using the model, we computed the vector potential and the horizontal and vertical components of velocity. The model generated the wind vectors as a function of position in a threedimensional field. As a diagnostic, we also computed divergence values; analytically, these are exactly zero since the rotational portion of a flow field is nondivergent. This diagnostic gave us a strong test of the correctness of the wind field, although the finite differencing we used yielded some small non-zero values.

Initially, the program was run with 3 rings at 3 km elevation and radii of 2.5, 3.0, and 4.0 km. These values were selected, along with ring circulation strengths of 120, 80, and 60 km-m/s, respectively, to generate near-surface peak velocities of 20-30 m/s, similar to those found with the microbursts studied by Fujita (1985) during the JAWS Project. The individual rotors could not be resolved and further examination of the model indicated that this flow was best interpreted as modelling the total flow pattern, including the return flow to the parent cloud, associated with the entire microburst.

Since the choice of *rings* did not actually model the near-surface rotor seen in observations, the emphasis on the three rotors at mid-levels in the atmosphere was replaced with emphasis on a single rotor closer to the surface. The vortex circulation strength for the higher rotors was set at 0.01 km-m/s, based on our evaluations of model runs at various strengths. We set the overall height of the return flow at 3 km, an average value for the height of the cloud base for high-based microburst-producing clouds, based on the microburst cases examined by Fujita (1985) from the JAWS and NIMROD Projects. The radius of each ring was adjusted to a value that, when combined with the near-surface rotor, modelled a flow which had velocities and flow fields similar to these flow fields. The mid-level rings were finally set at distances

of 3 km, 4 km, and 6 km, respectively, from the microburst center.

The near-surface ring was set at a radius of 2.5 km from the microburst center; the height of this rotor was set at 1 km. Most of the microbursts detailed by Fujita (1986) showed the rotor occurring between the surface and 1 km in height and 1 km to 2 km from the center of the microburst. In some cases, though, the stretching and expanding of this rotor extended the horizontal extent of the microburst farther than 4 km. Figs. 8-10, described below, show the flow we simulated. The flow is modelled along a 5-km by 5-km horizontal and vertical grid.

Fig. 8 displays a cut through the r-z plane of the vector potential amplitude for this flow. Corresponding streamlines for this pattern can be drawn parallel to these isopleths. The small extremum near the 2.5-km radius on the figure corresponds to the location of the near-surface rotor. Fig. 9 maps the streamlines for this flow. The location of the rotor is easily seen as well as the direction of the wind flow. In Fig. 10, the relative wind speeds associated with this flow can be seen; the length of the arrow corresponds to the wind speed at that position. The location of the near-surface rotor is also clearly evident. In addition, we can also see the wind speeds in the core of the microburst increasing with

descent towards the ground and as the wind flow spreads out at the surface.

We examined output detailing the calculated velocities used to model these flows and compared them to the velocity data published by Fujita (1986) on the 1985 DFW microburst. These data provided us the horizontal and vertical wind components, showing vertical and horizontal wind speeds of nearly 26 m/s associated with the microburst. We modelled horizontal and vertical wind components of up to 22 m/s, also our peak wind speed, associated with the microburst, which was also consistent with the microburst data published from the JAWS Project (Fujita, 1985).

We also compared our model to Ivan's (1986) model and Etkin and Zhu's (1986) model. We did this by running our model using the parameters Ivan used in his model and by using the parameters suggested by Etkin (1987) in his published comments on Ivan's work. Ivan's model examined a vortex at approximately 1 km (3000 ft) in height, a vortex radius of approximately 1.5 km (5000 ft) and a reference velocity at this height of 10 m/s (35 ft/s). The equivalent vortex circulation strength for Ivan's model was calculated to be 40.8 km-m/s. The pattern of vector potential amplitude for Ivan's model was very similar to the pattern we saw when our model was run for a

similar vortex radius and height, although the values for Ivan's model were smaller since his vortex strength was smaller. The streamline pattern produced by Ivan's model was also similar to our pattern under similar conditions, although the magnitudes of the winds were smaller because of the smaller vortex strength.

In his comments to Ivan's paper, Etkin (1987) suggested using 4 vortices, at 1 km elevation, with intensities of 100.0, 84.7, 56.7, and 19.9 km-m/s and radii of 1, 3, 5, and 7 km, respectively. Using these values in our model yielded very similar patterns of vector potential amplitude. The divergence values were larger than those for our model due to the stronger intensities of Etkin's rotors. Etkin's streamline pattern failed to show the individual vortex rings, including the strongest rotor at 1 km. This result reflects the merging of the velocity vectors of each rotor, acting to cancel each other. The surface horizontal wind speeds were similar, in the 20 m/s range, but covered a much larger area, which is also consistent with modelling several strong rotors spread over 7 km. The vertical winds near the center of the microburst were quite a bit stronger, with several values in the 30-47 m/s range. At 53 m/s, the peak wind speed was much larger than the peak wind speed associated with the our flow pattern. However, given the similarity of the flow patterns, even with the

different circulation strengths used by Etkin and Ivan, the output of our modelled flow looks reasonable.

3. RESULTS

As mentioned in the introduction, we assumed axial symmetry, uniform beam-filling, and time independence for the microburst. In examining the horizontal and vertical velocities generated by our model, we had two options. The first was to calculate the 3-dimensional velocity at each point, a time-consuming and expensive proposition. The other option, which we selected, was to examine the microburst flow along a verticallyaveraged horizontal profile, calculating the velocities over a grid. We selected a 5 km x 5 km grid, with grid spacing every 0.25 km, yielding a 20 x 20 point matrix of microburst velocities.

We averaged these velocities over the lowest 0.5 km of the modelled flow to create the horizontal profile of vertically-averaged microburst velocities, $\bar{V}$, accounting for the vertical smoothing produced by the radar. We chose the lowest 0.5 km as representative of the layer which Wilson, et al. (1984) suggested should be covered. When necessary, we extrapolated past 5 km in the horizontal to determine velocities out to the point where the microburst velocity fell to zero. The extrapolation was a reasonable approach since the velocities were already small at 5 km. The velocities were then saved to a file for use in computing the Doppler velocities.

As we prepare to compute the Doppler velocity for any point in the microburst flow (Fig. 11), we know the direction and distance from the radar to the point in question ($\vec{RR}$), the direction and distance from the radar to the center of the microburst ($\vec{R}$), and the azimuth angle (θ). Knowing these variables, we can use the Law of Cosines to determine the relative position ($\vec{r}$) from the center of the microburst to the point in question:

$$\vec{r} = (\vec{RR} + \vec{R} - 2(\vec{R})(\vec{RR})\cos\theta). \qquad (9)$$

With this information, we can solve for the angle Φ, the angle created by the microburst velocity and the radial from the radar:

$$\Phi = \sin((|\vec{R}|/|\vec{r}|)\sin\theta). \qquad (10)$$

The Doppler velocity is the projection of the microburst velocity to the radar radial. Knowing Φ, we determine the Doppler velocity for any point of interest:

$$\vec{V}_D = \left(\vec{V} \cdot \frac{\vec{RR}}{|\vec{RR}|}\right)\left(\frac{\vec{RR}}{\vec{RR}}\right) = |\vec{V}|\cos\Phi\ \frac{\vec{RR}}{\vec{RR}}. \qquad (11)$$

Knowing the distance of the point of interest from the center of the microburst, we go to that location on the horizontal velocity profile, interpolating or extrapolating as necessary to calculate $\vec{V}_D$. The Doppler velocities were used to create the velocity-based

parameters we used to investigate the capabilities and limitations of a single Doppler radar.

In evaluating how a Doppler radar views a microburst, we needed to examine many points in the microburst flow. We calculated the Doppler velocity for a particular range bin and azimuth angle by computing the Doppler velocities for azimuth angles every 0.1 deg extending to 0.5 deg on either side of the specified azimuth angle. Each range bin was 0.25 km long. Since the radar antenna pattern is a Gaussian distribution, which means the transmitted and returned signals are Gaussian distributions, we weighted the Doppler velocities using a 9-point Gaussian-squared distribution that assigned the greatest weight to the center velocity value and lesser weights to the off-center magnitudes (Table 1). Using this technique, we were able to examine microburst velocities for different azimuth angles and different ranges. The velocites were computed with the conventional algebraic sign for motion towards the radar (negative) or away from the radar (positive).

The Doppler velocities were used to determine the maximum velocities towards and away from the radar and the ranges at which these occurred. In addition, the difference between the maximum towards and away velocities, the radial shear, was calculated. These parameters were all calculated with respect to a range of

azimuth angles where the 0-deg radial extended to the center of the microburst. As expected, the maximum towards/away velocities for any "mirror" azimuth angles (e.g., 0.5 deg and -0.5 deg) were equal and occurred at the same distances from the center of the microburst.

The peak in the Doppler velocities occurred for an azimuth of zero degrees, as expected since at this azimuth the radar beam is parallel to the flow. These velocities decreased with increased azimuth angle, as expected (Fig. 12). The peak magnitude for each range value decreased with azimuth angle; the differences became even larger as the azimuth angle increased. When the range of the microburst center from the radar is doubled from 15 km to 30 km, the difference between the magnitudes of maximum towards velocities, or maximum away velocities, at an azimuth angle of 3.0 deg off the center of the microburst is about 2.5 m/s (Table 2) due to beam spreading. This difference means the radial shear at 30 km is about 5 m/s less than the radial shear at 15 km along the 3-deg beam.

Since the azimuthal sampling for the NEXRAD system will be done every one degree, the question that's really important is how the velocities differ over the 1-deg beam. Since the beam samples to 0.5 deg to either side of the center value, the maximum offset will be 0.5 deg. To determine the effect of the offset, we calculated the

parameters for azimuth angles every 0.1 deg over a 1-deg azimuth angle. The parameters for eac 0.1-deg increment were calculated as before by determining the values for every 0.1 deg over a range of 0.5 deg on either side of this angle. The parameters calculated were the magnitudes of the maximum towards velocities, the radial shear, and the radial shear normalized by the difference in range between the maximum towards and away velocities. Table 3 displays the data and Figs. 13-15 illustrate the points described below.

At an azimuth offset of 0.5 deg, the beam is as far off center as possible. So even though we calculated the parameters for azimuth angles out to 1 deg, the pertinent information is for the data at azimuth angles of 0.5 deg and smaller. Each of the parameters shows the same pattern. For a microburst 15 km from the radar, the difference in the values over each 0.1-deg increment is extremely small; over the entire 0.0-0.5 deg range it is only 0.03 m/s between the magnitudes of the maximum towards (or away) velocities, a difference so small as to be negligible. As the distance of the microburst from the radar increases, the difference in magnitude over each azimuth angle increases also. At 30 km, the difference is only 0.12 m/s between the maximum towards (or away) velocity values at the 0 deg and 0.5 deg azimuths (Fig. 13). At 60 km, this increases to about 0.47 m/s

difference between these values, or about 0.95 m/s difference in the radial shear (Fig. 14). The same pattern holds for the normalized velocities (Fig. 15). These results show that at longer distances, portions of the microburst viewed only a few tenths of a degree off center will have velocity magnitudes that are underestimated from their true values, but the magnitudes of these differences are so small as to be negligible.

3.1 The Effects of Smoothing

Smoothing of data for ranges less than a specified range can cause the peak value of the variable to be missed. The amount of smoothing depends on the range to which the returns are smoothed. We wondered what effects smoothing would have on microburst data for ranges less than the specified range if smoothed to the resolution of the data at the longer range. Considering the standard 1-deg beamwidth (θ = 1 deg) as a constant, its width at 30 km (= R) from the radar is given by

$$L = R\,\theta \qquad (12)$$

where L is the arc length in km, or an arc length of 0.5 km. Using 0.5 km as the size of the averaging volume, we compared smoothed and unsmoothed velocity-based data for several microbursts centered at distances of less than 30 km.

To do this comparison, we established a fixed grid box with a center arc of 0.5 km and sides of 0.5 km, 0.25 km to either side of the center arc (Fig. 16). If we move the grid box closer to the radar, the azimuth angle subtended by the grid box increases; the azimuthal angle sampled over would be larger than one degree. Thus, a microburst viewed at this closer range would experience additional smoothing than it would at 30 km. After calculating the upper and lower azimuthal boundaries for the grid box at each range, when the boundary angle fell between two of the azimuth angles in the data file, we computed a weighted velocity value, weighted by the fraction of the range bin included in the box, to determine the contribution of the partially represented range bins. The amount of difference between smoothed and unsmoothed velocity values varies as the grid box changes along the range.

Considering a microburst centered 15 km from a Doppler radar, we examined the smoothed velocities from 9 km to 21 km with 0.25 km range gates in distance and azimuth angles from 0 deg to +/- 5 deg (Fig. 17). Although the overall effects of the smoothing were small (compare with Fig. 12), we saw the expected flattening of the peak velocity value (by about 0.2 m/s); this occurred at a range of about 17 km and 0 deg azimuth, the location of the near-surface rotor when the center of the

microburst is located 15 km from the radar. The difference in the smoothed velocities between 0 deg and 5 deg azimuth is only about 2 m/s.

We also compared the smoothed velocities with the unsmoothed velocities as a function of azimuth angle and range. For this case we examined microbursts centered 10 km, 15 km, 20 km, 25 km, and 30 km from the radar. The differences between smoothed and unsmoothed velocities for azimuth angles up to about 5 deg was less than 0.4 m/s for most ranges with a maximum of 0.6 m/s occurring where the near-surface rotor influence begins to dominate. For radial shear, an important parameter in microburst detection, we see in Figs. 18 and 19 little difference between the maximum radial shear at a given azimuth for these microbursts. Even for the microburst 10 km away (Fig. 18), where one would expect the greatest difference between smoothed and unsmoothed values as the microburst data is smoothed to 30 km, the differences are less than 1 m/s. However, these calculations do not take into account radar "blanking", an area 8 km (5 mi) in radius closest to the antenna which is not able to be viewed due to the antenna height above the ground.

We also examined the differences between smoothed and unsmoothed velocities at azimuth angles between 0 and 1 deg. Keeping the arc length (L) fixed at 0.5 km, we

divided the beam into 0.1-deg increments, determining the value for every 0.01 deg over a range of 0.05 deg on either side of the increment. Over the entire range of azimuths from 0.1 to 1.0 deg, the difference between the smoothed and unsmoothed velocities never differed by more than 0.8 m/s with most differences less than 0.5 m/s. This represented differences from 2% to 5% between smoothed and unsmoothed velocities. The largest differences occurred at the point of the near-surface rotor's influence, as before. Comparing the maximum radial shears for smoothed and unsmoothed Doppler velocities for each azimuth angle (Fig. 20), the largest differences were only about 1.3 m/s, about a 4% difference. These values are similar to those calculated for a beam covering 1 deg in azimuth, indicating that those values can be considered fairly accurate. These results indicate the effects of smoothing should be minimal for the TDWR and NEXRAD programs since both programs will have a 1-deg azimuth sampling rate.

3.2 The Effects Over Very Long Distances

The results for the smoothed cases made us wonder just how far one could go away from the radar before the signal became too degraded to be useful. So we decided to look at the effects on unsmoothed velocity data of increasing the microburst distance from the radar and increasing the azimuth angle.

Looking first at a microburst 15 km from the radar, we examined azimuth angles at 0, 3, 5, 7, and 9 deg (Fig. 21). Very little difference was seen in the Doppler velocities between 0 deg and 3 deg (see Fig.12). After this point, the differences were more noticeable (Fig. 21), with a 10 m/s difference between the Doppler velocities between 0 deg and 9 deg at the location of the near-surface rotor 2.5 km from the center of the microburst.

Expanding upon this to look at microbursts 15, 20, and 30 km from the radar at azimuth angles of 0, 5, and 7 deg (Fig. 21), we saw no difference in the detected maximum away velocity magnitudes at 0 deg azimuth at any of the ranges. However, there is a definite decrease, due to beam spreading, in the maximum velocity values detected with increasing azimuth angle and increasing range. We found the same results for the maximum velocity towards the radar.

To see the effect of range on the velocities viewed up to 0.5 deg offset from the center of the 1-deg beam, we looked at microbursts centered up to 150 km from the radar. Table 3 provides the data for cases from 15 km to 150 km. Using the 15-km microburst as a standard, for a 0 deg azimuth we see a difference of less than 1 m/s in the radial shear at 120 km and 1.5 m/s difference at

150 km. Comparing the radial shear for the 0.5-deg offset angle at 120 km and 150 km to the radial shear at 15 km for a 0 deg azimuth, we see a difference in the radial shear of 4.28 m/s at 120 km and 6.39 m/s at 150 km, a difference of 12% and 18%, respectively, from the 35.423 m/s value at 15 km and 0 deg azimuth. These are sufficiently large differences that users might draw incorrect conclusions from the quantitative parameters.

To determine the maximum and minimum velocities one would see for a microburst viewed at these longer ranges, we compared values for the 0 deg to 0.5 deg azimuths in Table 3 (Fig. 23). For a microburst centered at 120 km, the difference in radial shear is 3.3 m/s, a 10% difference. For a 150-km microburst, the difference is 4.89 m/s, a 14% difference. So the microburst signature will vary 10-15% just in the 0.5 degrees it is sampled over in the azimuth. Therefore, a maximum fluctuation of 10-15% in the quantitative parameters chould be expected due to this uncertainty. More likely, though, the fluctuation will be smaller since the returns to the radar, for each 1-deg wide beam, are averaged over 1-deg wide range bins. Even so, microbursts having a near-surface rotor with a radius smaller than the 2.5 km radius we used will experience these fluctuations at proportionately shorter distances. All of these

considerations must be taken into account when developing the NEXRAD/TDWR software to evaluate the radar returns.

This leads us to conclude that in using a Doppler radar to continuously interrogate a microburst, the microburst must fall directly on a radial, with a 0 deg azimuth being ideal, to detect the full magnitude of the Doppler velocities, especially at greater distances from the radar. This is very unlikely since NEXRAD is planned to scan almost exclusively in an automated mode.

3.3 The Parameters as a Function of Arc Length

We considered that examining the parameters as a function of arc length might reveal the structure of the parameters more clearly than examining them as a function of azimuth since the azimuth angle cuts through the microburst differently at different ranges. For example, an arc length of about 5.75 km corresponds to an azimuth angle of 11 deg for a 30-km microburst but only 5.5 deg (half the value) for a 60-km microburst (twice the distance). We decided to examine Doppler velocity parameters as a function of arc length. The parameters we chose to use, plotted against arc length, were:

1. The radial shear (the difference between the maximum towards and away velocities), plotted as delta-Velocity,

2. The difference between the maximum radial shear (the radial shear for the 0 deg azimuth angle) and the radial shear, plotted as del-Velocity, and,

3. The normalized velocity, the quotient of del-Velocity divided by the maximum radial shear, plotted as max del-Velocity.

Using these parameters, we plotted the results for a microburst centered at 30, 40, 50, and 60 km from the radar (see Table 4 for data). Figs. 24-26 show very little difference in the parameters, even out to 60 km. The greatest difference between values of del-Velocity (the difference between maximum radial shear and the radial shear at that arc length) was only about 1 m/s for microbursts centered at 30 km and 60 km.

We increased the range to 150 km, looking at microbursts centered at 30 km, 90 km, 120 km and 150 km from the radar (see Table 4 for data). Figs. 27-29 and 30-32 illustrate our results; note that max del-Velocity is plotted as the normalized Doppler velocity.

Comparing data for the same arc lengths, we see that for an arc length of 4.188 km, the radial shear at 30 km, 60 km, 120 km, and 150 km is 3.08 m/s, 3.15 m/s, 3.61 m/s, and 3.99 m/s, respectively. This represents a difference

of 2%, 17%, and 30%, respectively, from the value at 30 km. For an arc length of 1.047 km, the radial shear is 31.787 m/s, 31.663 m/s, 31.147 m/s, and 30.749 m/s, respectively. For this arc length, this is a difference of less than 1%, 2%, and 3%, respectively, from the value at 30 km. For smaller arc lengths, the differences are small and can be ignored. But as arc length increases, the differences also increase and corrections must be made. This is not surprising, though, since at arc lengths of about 4 km the velocity is changing rapidly with arc length and details of averaging might matter.

4. DISCUSSION AND CONCLUDING REMARKS

We examined velocity parameters calculated from a simulated microburst flow to determine the effects of azimuth angle and range on the quality of the signal returned to the radar. Using cases of microbursts centered at 15 km and 30 km from a single Doppler radar, we examined maximum towards and away velocities, the radial shear and the normalized radial shear for a given range and azimuth angles up to 5 deg. We saw a decrease in maximum towards (or away) velocities of about 2.5 m/s, so a difference in the radial shear of about 5 m/s, for a microburst viewed from 30 km away at an azimuth angle of 3 deg off the center of the microburst. As the azimuth angle increases beyond this point, the magnitudes of the detected radial velocity parameters decline rapidly since the angle between the velocity and the radar radial is also increasing. For a weak microburst, this means the total area impacted by the microburst could be hard to determine. The planned azimuthal sampling of every 1 deg for NEXRAD lessens this concern unless algorithms are developed that require information gathered at azimuth angles larger than a few degrees off the center of the microburst.

Because a microburst can exist at any azimuthal angle, we also examined the magnitudes of the maximum

towards and away velocities, the radial shear, and the radial shear normalized over the distance between the maximum towards/away velocities for azimuth angles between 0 and 1 deg in 0.1-deg increments. Here we again saw a decrease in the parameters as a function of azimuth angle and increased distance of the microburst from the radar. The difference for a microburst centered at 60 km only amounted to about 0.95 m/s, a difference of about 3%, for the radial shear between 0 deg and 0.5 deg azimuth, the maximum offset for each 1-deg sample in the azimuth. These differences increased with range. For a microburst centered at 120 km, the difference was about 3.3 m/s, a 10% difference. For a microburst centered at 150 km, the difference was about 4.89 m/s, a 14% difference. Compared to the radial shear at 15 km for an azimuth of 0 deg, the differences were 4.28 m/s (12%) at 120 km and 6.39 m/s (18%) at 150 km. This tells us that the velocity parameters examined at the edges of the beam will be smaller than their true values. The averaging done over the whole beam will decrease the differences, but there will still be differences between the true wind speeds and those perceived by the radar. For microbursts with a near-surface rotor of a radius different from the one we modelled, these differences will occur at ranges proportionate to the difference in size between the two rotors. If not corrected in the NEXRAD/TDWR software, a microburst will appear to fluctuate in strength and wind

speed depending on its exact position within the radar beam.

We also examined the effects of smoothing on velocity-based parameters smoothed to 30 km for microbursts centered at closer distances to the radar. By developing a 0.5 km by 0.5 km grid box, corresponding to the arc length subtended by a 1-deg beam at 30 km, we studied microburst cases centered at 15 km, 20 km, and 25 km from the radar. The differences between the smoothed and unsmoothed velocity magnitudes were less than 1 m/s for azimuth angles up to 5 deg. For azimuths ranging from 0 to 1 deg in 0.1-deg increments for a microburst centered at 15 km, the differences were only slightly higher. This demonstrated the minimal effect of smoothing on the data.

Finally, we examined the radial shear, the difference between this shear and the maximum radial shear, and this difference normalized over the radial shear, all as a function of arc length, for microbursts centered at distances of up to 150 km from the radar. At shorter arc lengths, the differences were less than 5% in radial shear values for microbursts centered from 30 km to 150 km from the radar. For longer arc lengths, the percentage difference rose to about 30%, although this was because

the actual values for the radial shears were very small, in the 3 m/s range.

From these results, we can conclude that range alone has no significant effect on the usual microburst velocity parameters detected by a Doppler radar. Jendrowski's (1986) work showed changes in velocity-based parameters for mesocyclones because the information which can be determined from a mesocyclone lies in the azimuthal direction; azimuthal smoothing introduced by range has an important effect on the retrieval of mesocyclone parameters. But microbursts are detected from information which has its structure in the radial direction, so only small changes are seen simply due to range. At non-zero azimuth angles, range eventually has a strong effect on the velocity parameters, but the effect is due to beam spreading. For a 1-deg beamwidth, the azimuthal sampling angle planned for the NEXRAD and the TDWR systems, the effects are small. The information captured by the outer edges of the beam will induce error in the parameters which increases with range, up to a maximum 15% at a range of 150 km for a microburst with a near-surface rotor at 2.5 km, but this should be easily correctable in the NEXRAD/TDWR software since the degradation in the signal due to beam spreading shows a graceful decline with increasing range.

This study only addressed the effects of smoothing and finite sampling on a radar's capability to detect targets. The effects of the Earth's curvature were not included; neither was the problem of ground clutter considered. Clutter suppression techniques will be helpful in solving the ground clutter problem, but will not totally solve it. The uniform beam-filling assumption we used for simplicity is not always valid; a study where non-uniform beam-filling was a consideration could yield interesting information about the velocity returns a Doppler radar would see. The effects on the Doppler spectrum of turbulence and receiver noise were also not considered. These may be areas for further study.

In addition, further study is needed on mid-level microburst precursors such as rotation and convergence. Study in these areas could provide valuable advance warning and time to take action for both aviation and ground-based activities.

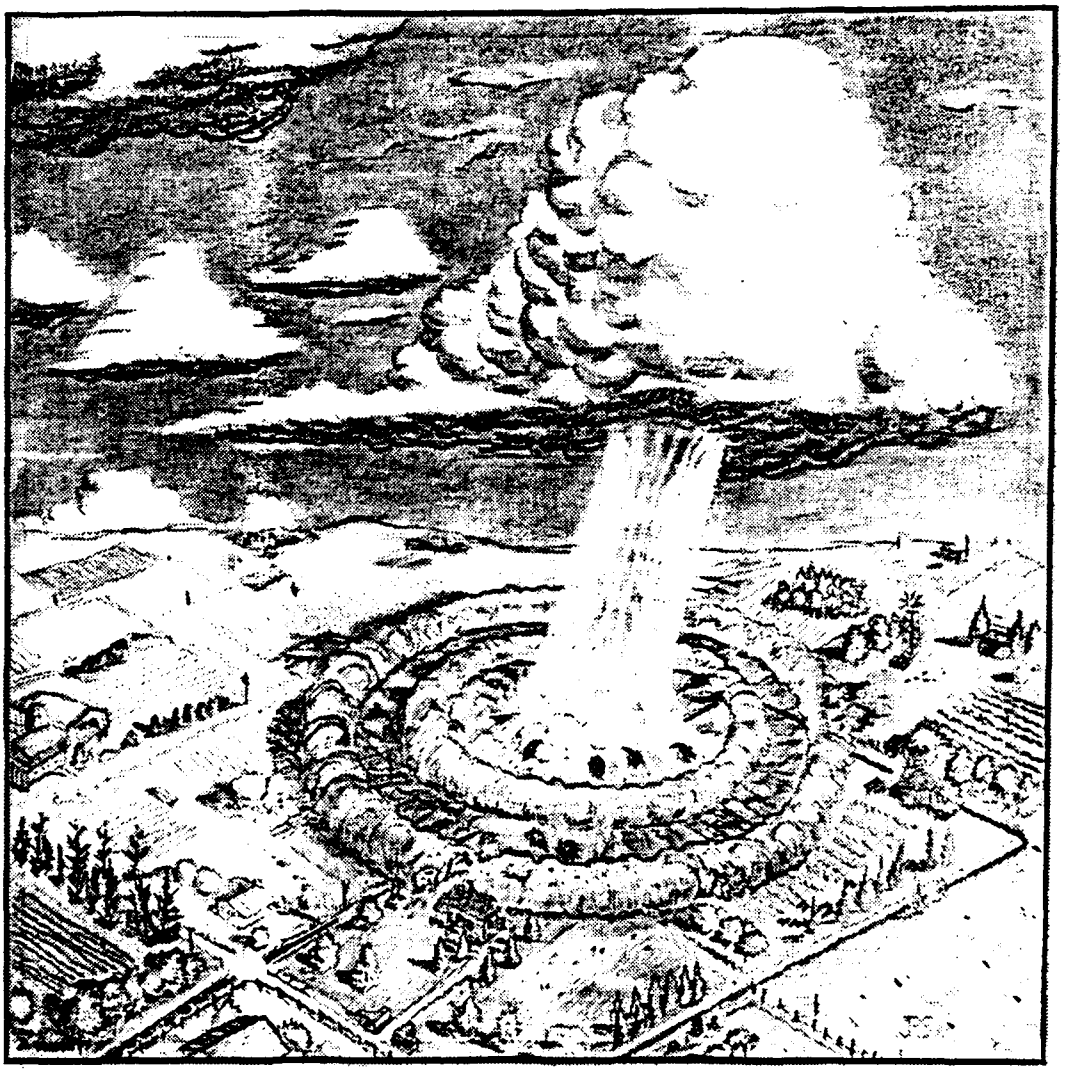

Figure 1. An artist's conception of a microburst. (Courtesy of Jeffrey Straight.)

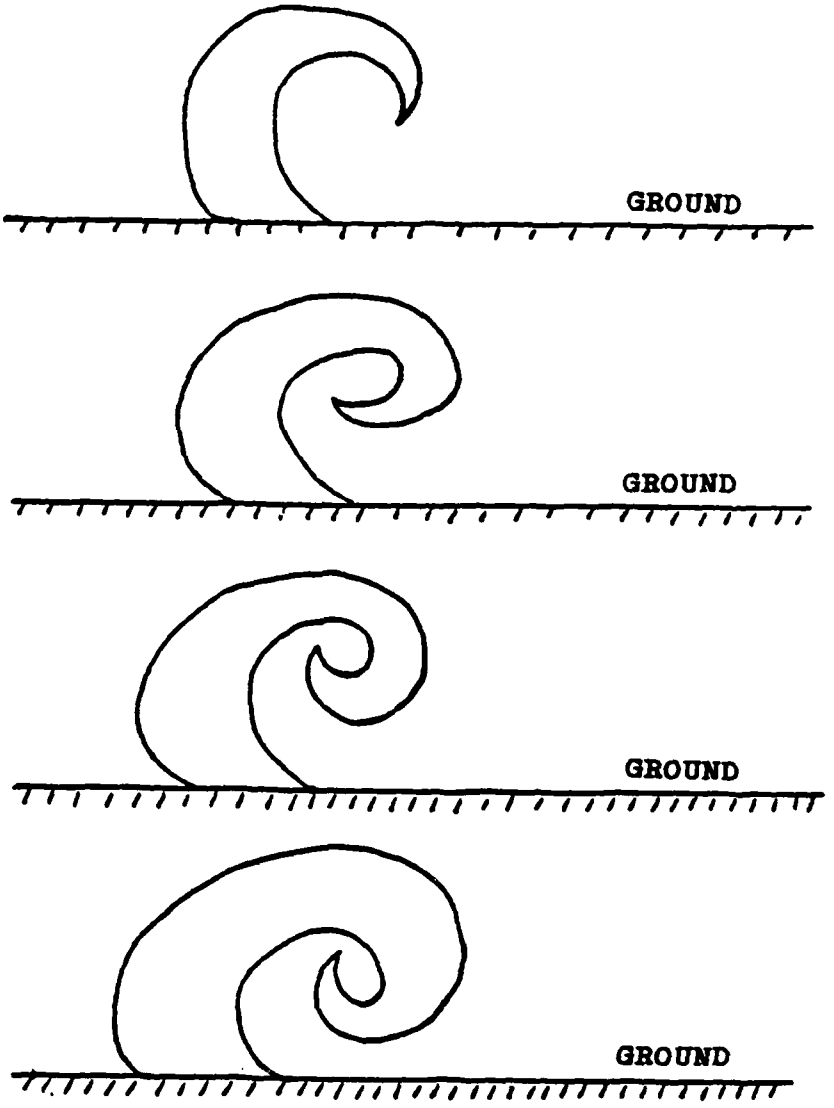

Figure 2. An idealized representation, from top to bottom, of the curling of the horizontal vortex. Total lapse time from top to bottom is on the order of 15-20 seconds. (Adapted from Andrews AFB Microburst. Six minutes after the touchdown of Air Force One, by T.T. Fujita, 1983, SMRP Research Paper 205.)

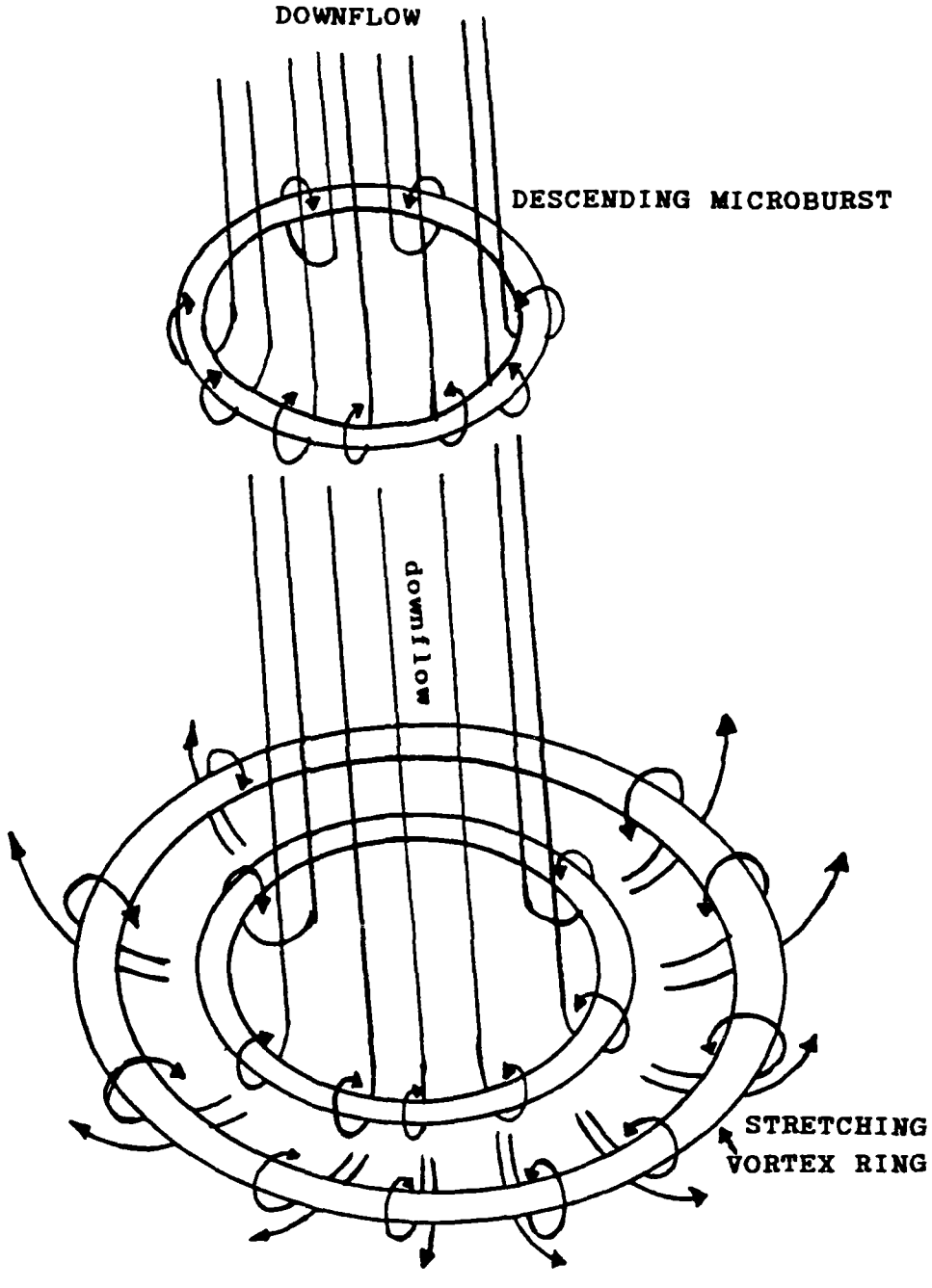

Figure 3. The stretching and expansion of microburst vortex rings. (Adapted from Andrews AFB Microburst, Six minutes after the touchdown of Air Force One, by T.T. Fujita, 1983, SMRP Research Paper 205.)

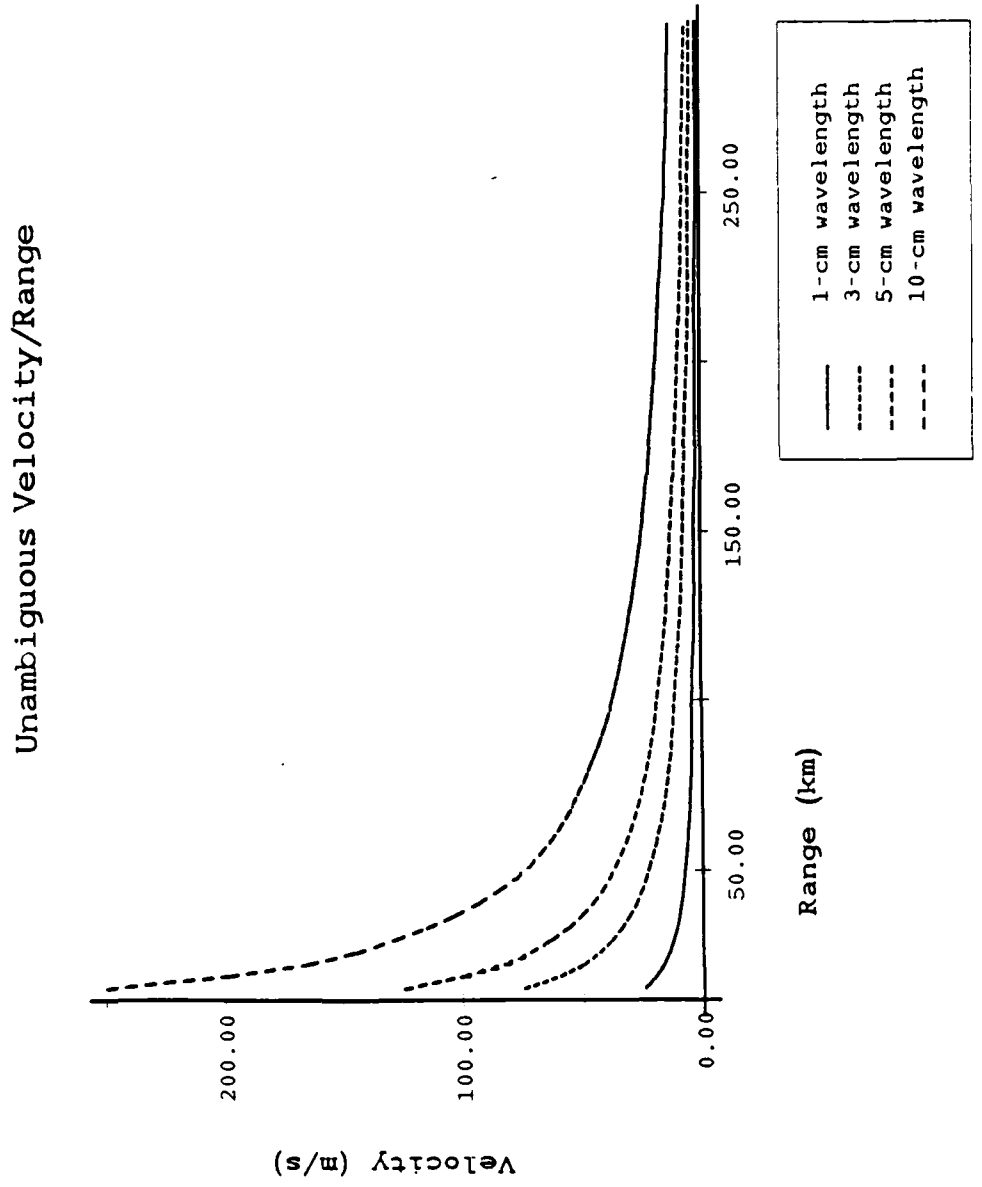

Figure 4. The trade-off between velocity and range for several wavelengths.

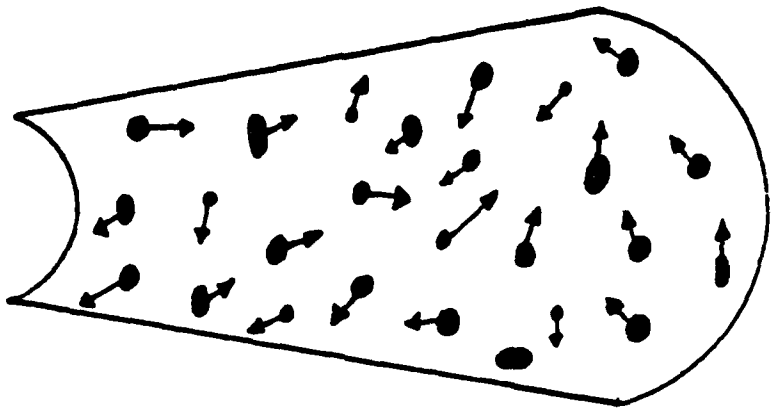

Figure 5. The echo volume of a pulsed radar beam - one beam width in cross-section and half a pulse length in length.

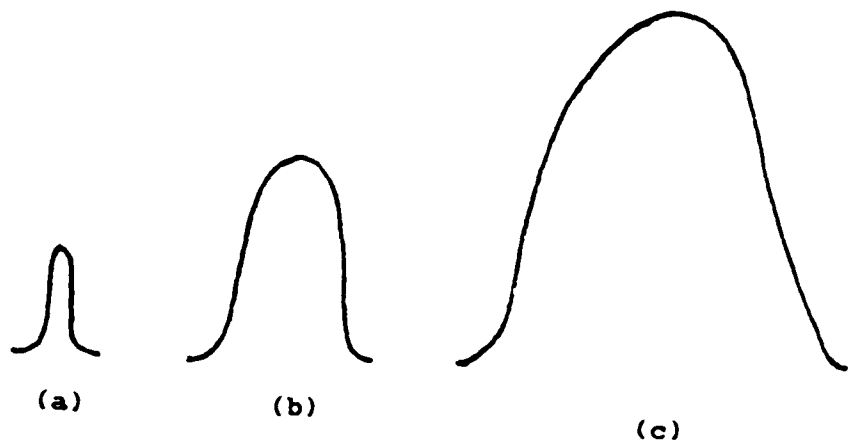

Figure 6. The comparative relationship between the Doppler spectrum width and a turbulent atmosphere as a function of the target character where (a) is light stratiform rain, (b) is a rain shower, and (c) is a thunderstorm.

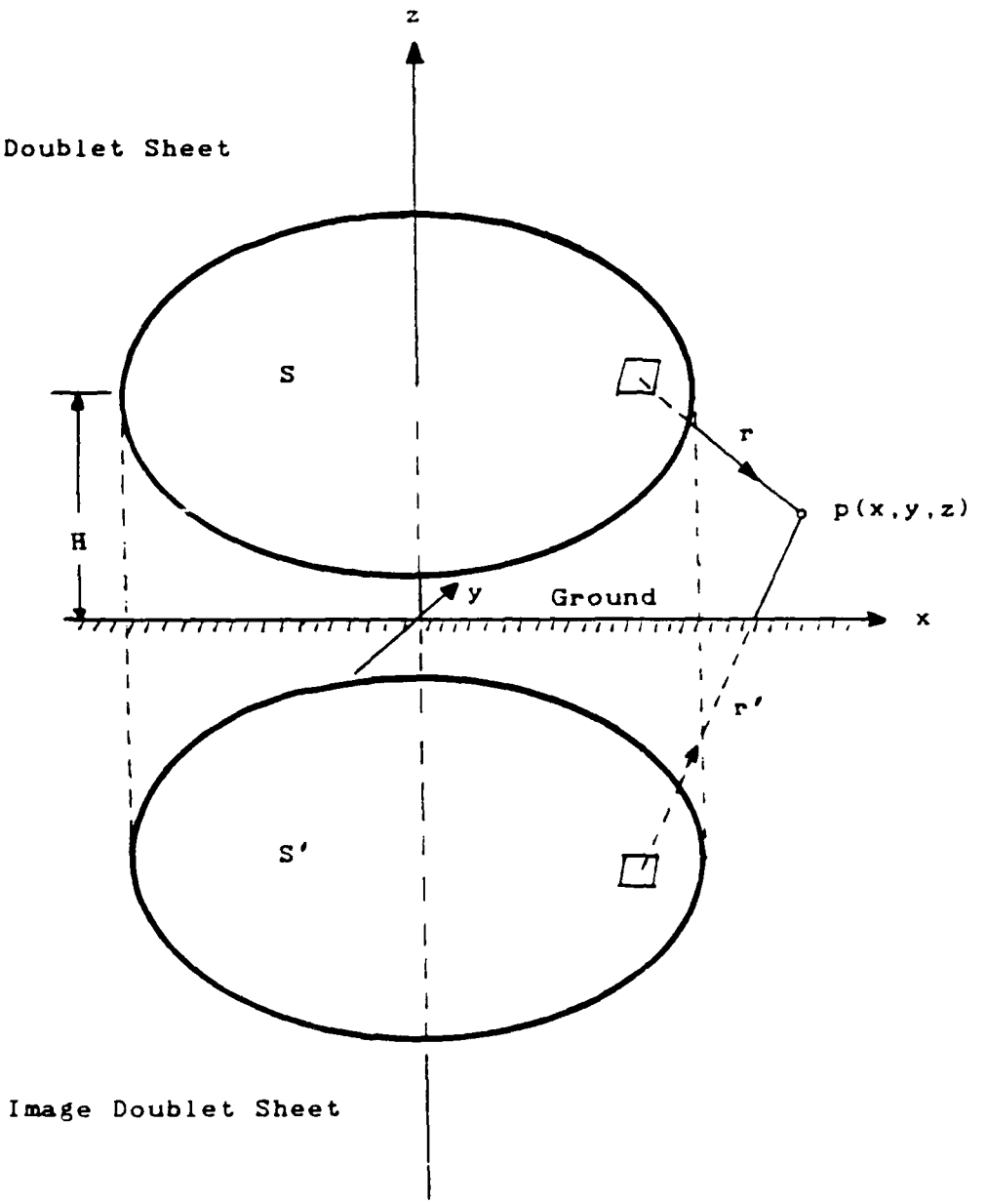

Figure 7a. Three-dimensional doublet sheet model. (Adapted from Model of the Wind Field in a Microburst, by S. Zhu and B. Etkin, 1985, J. Aircraft, 23, p. 596.)

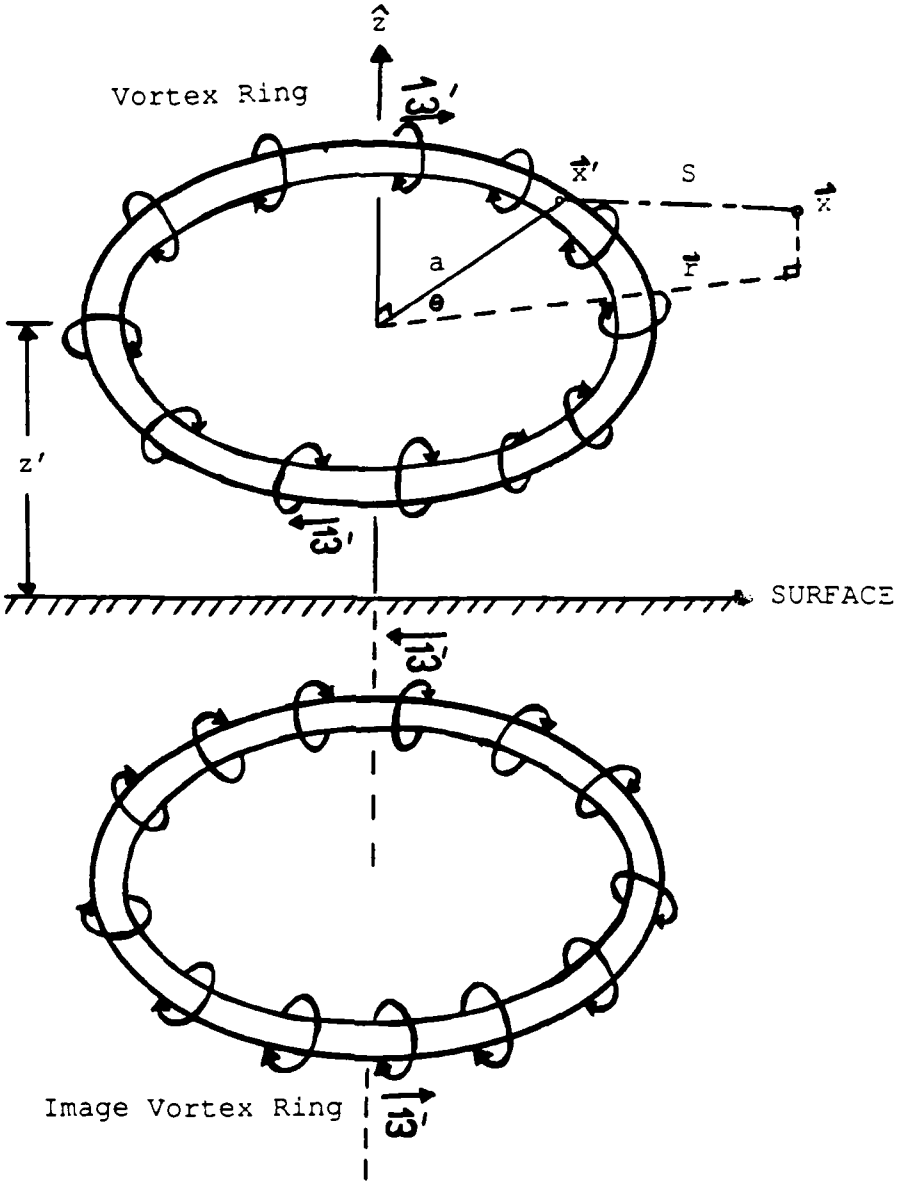

Figure 7b. Three-dimensional vortex ring model.

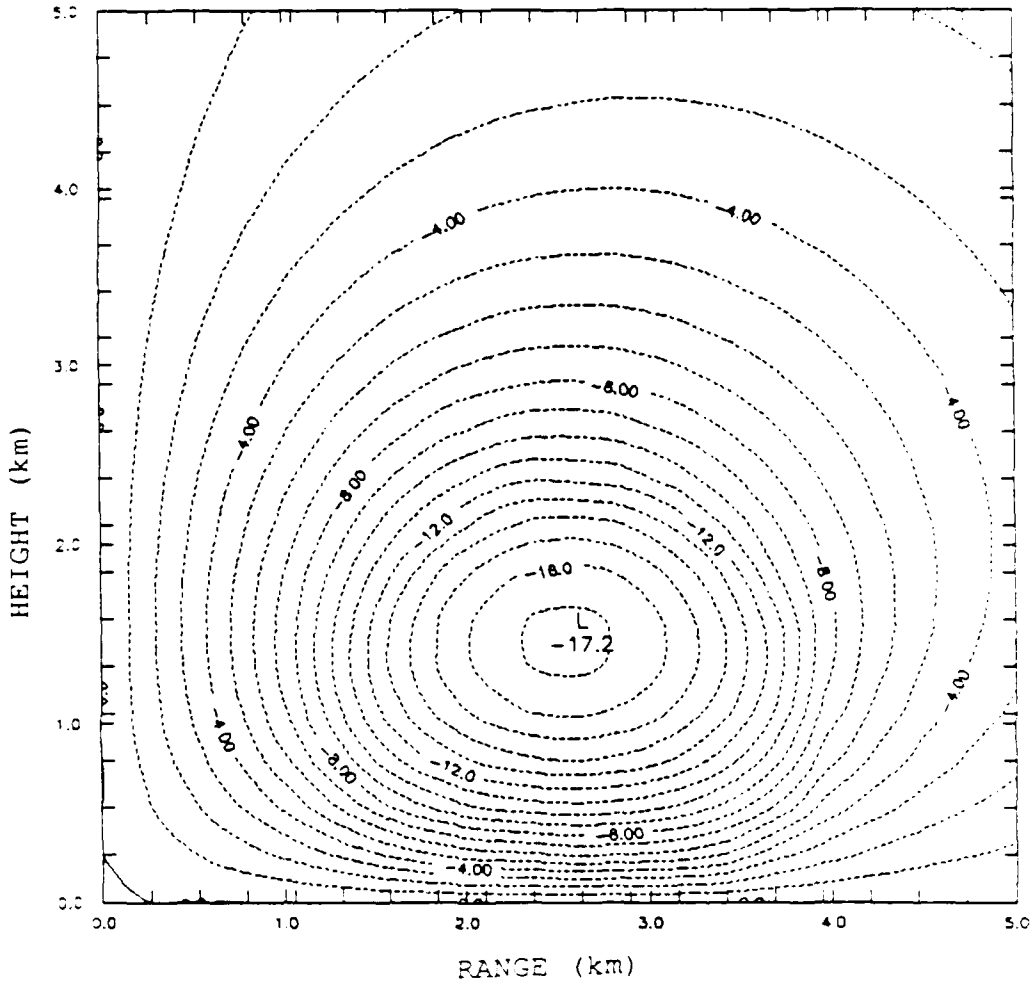

Figure 8. Map of the vector potential for the selected microburst flow.

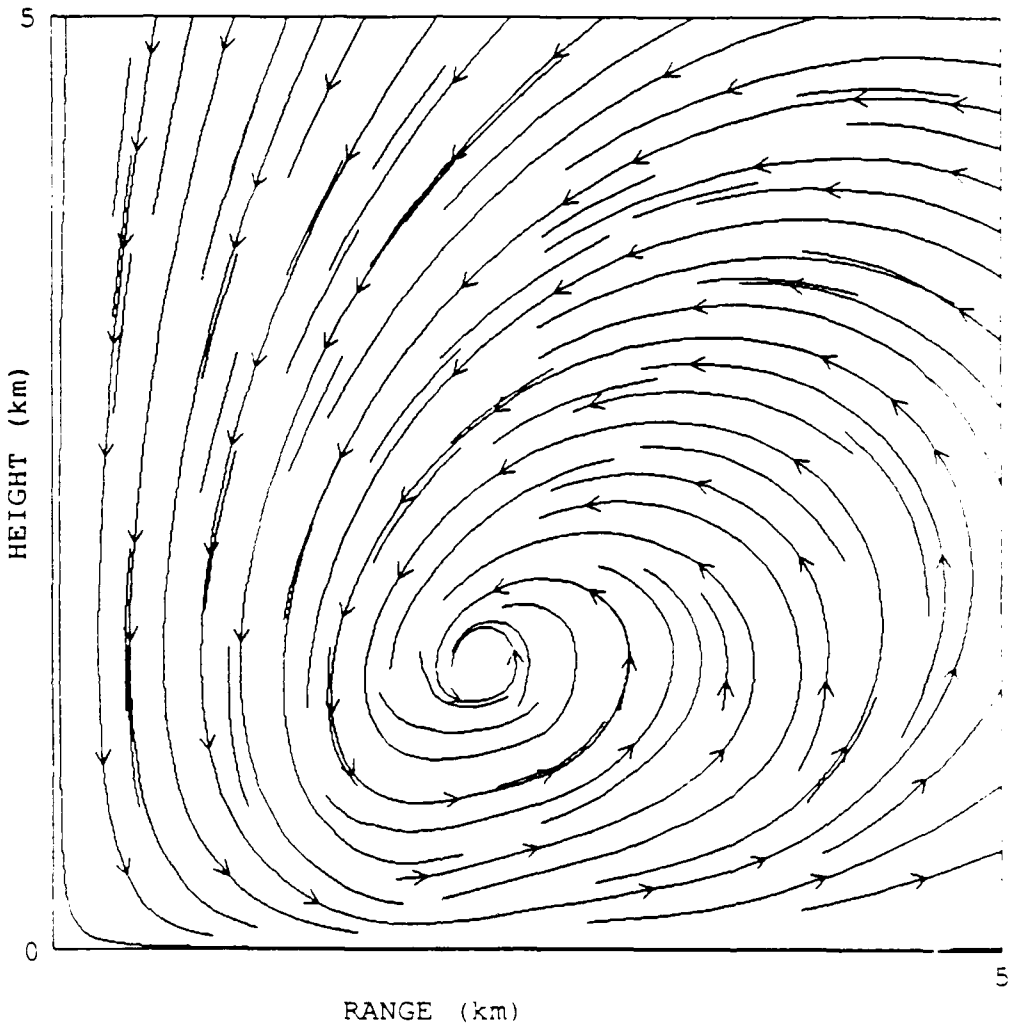

Figure 9. Map of the streamlines associated with the selected microburst flow.

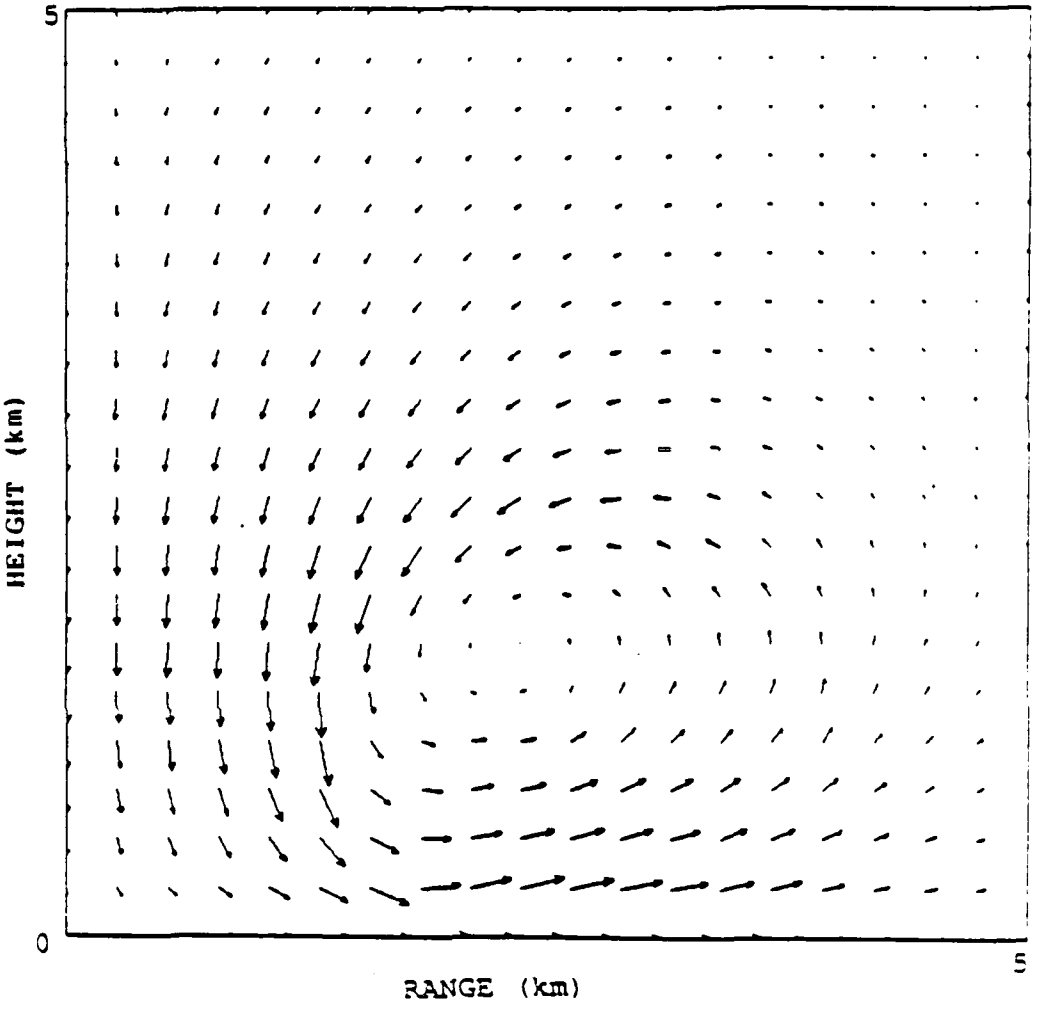

Figure 10. Map of the relative wind vectors, size of the arrow corresponding to relative speed, for the selected microburst flow.

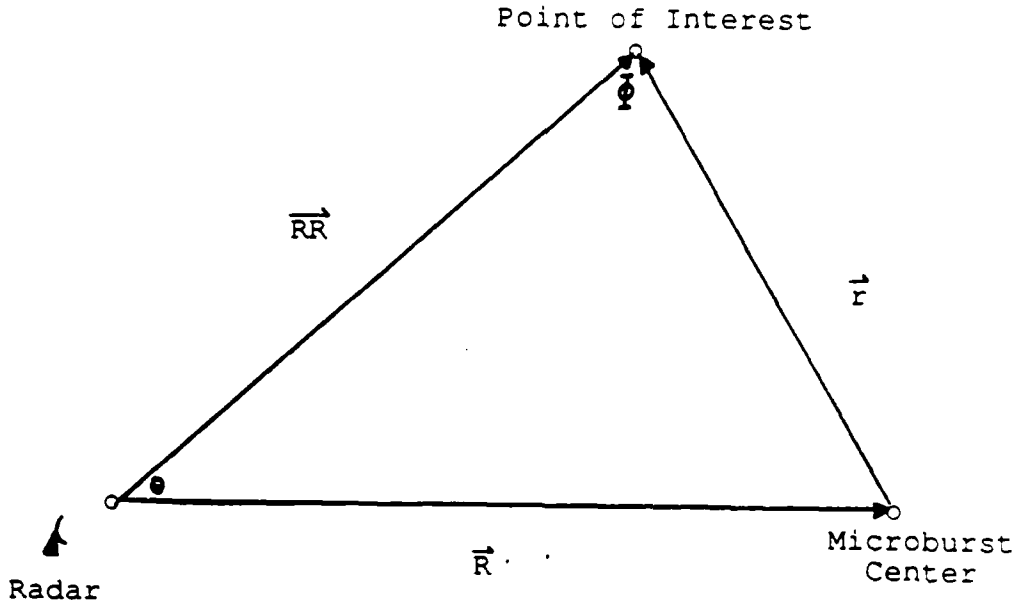

Figure 11. A diagram showing how the Doppler velocity was computed for any point in the microburst flow.

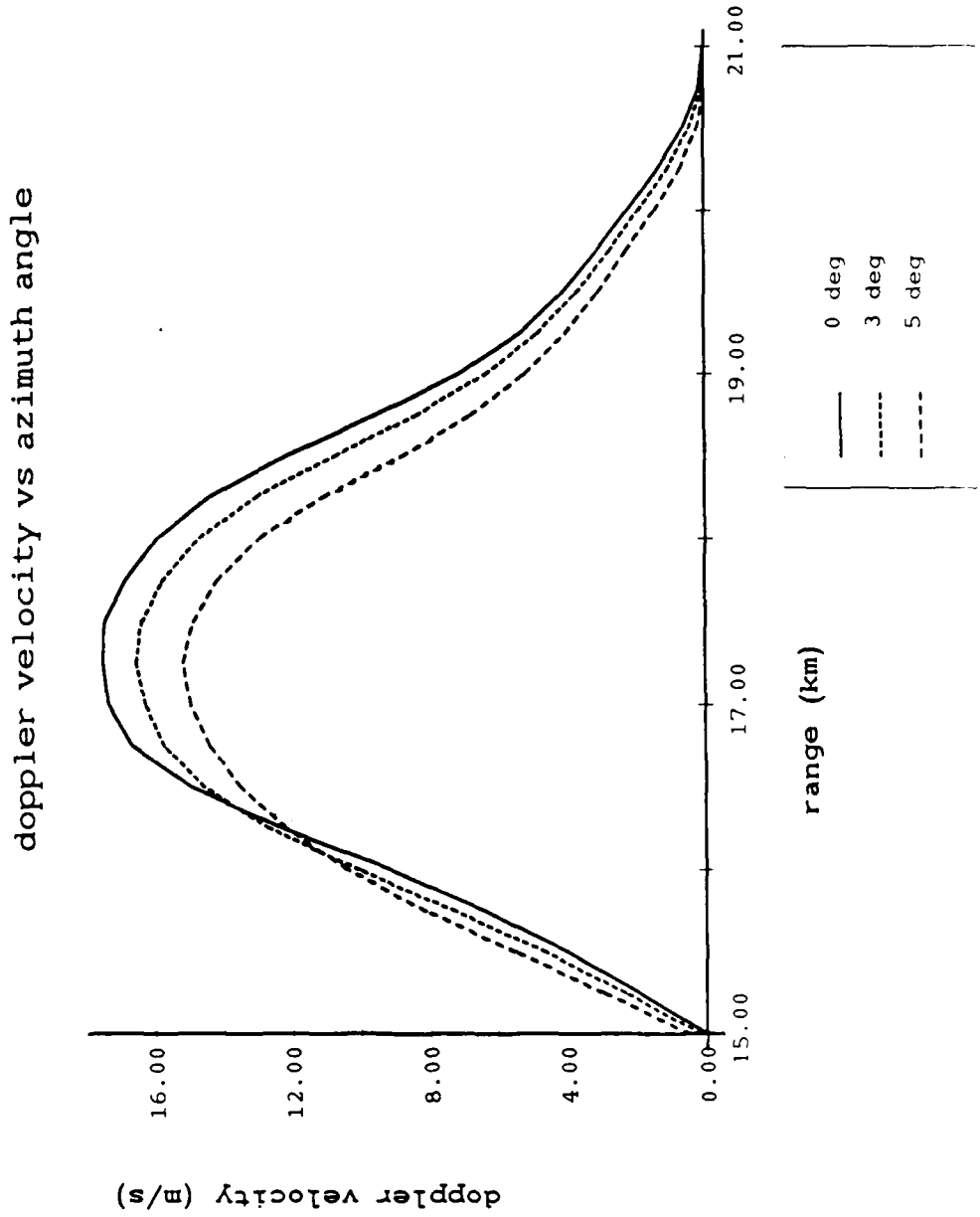

Figure 12. The peak Doppler velocities as a function of azimuth angle and range for a microburst with its center 15 km from a single Doppler radar.

Figure 13. Maximum radial Doppler velocity plotted against azimuth angle for a microburst with its center 15, 30, and 60 km from a single Doppler radar.

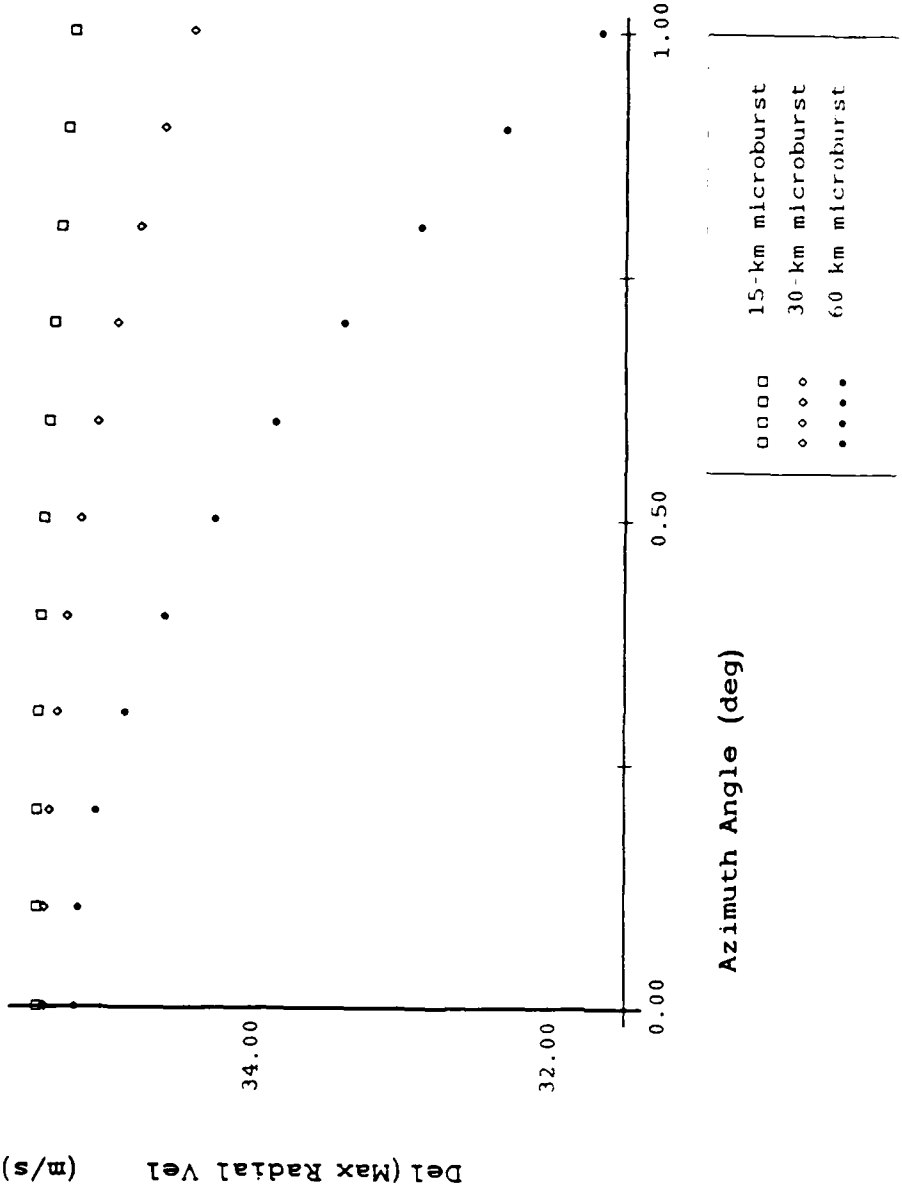

Figure 14. Radial shear plotted against azimuth angle, as in Fig. 13.

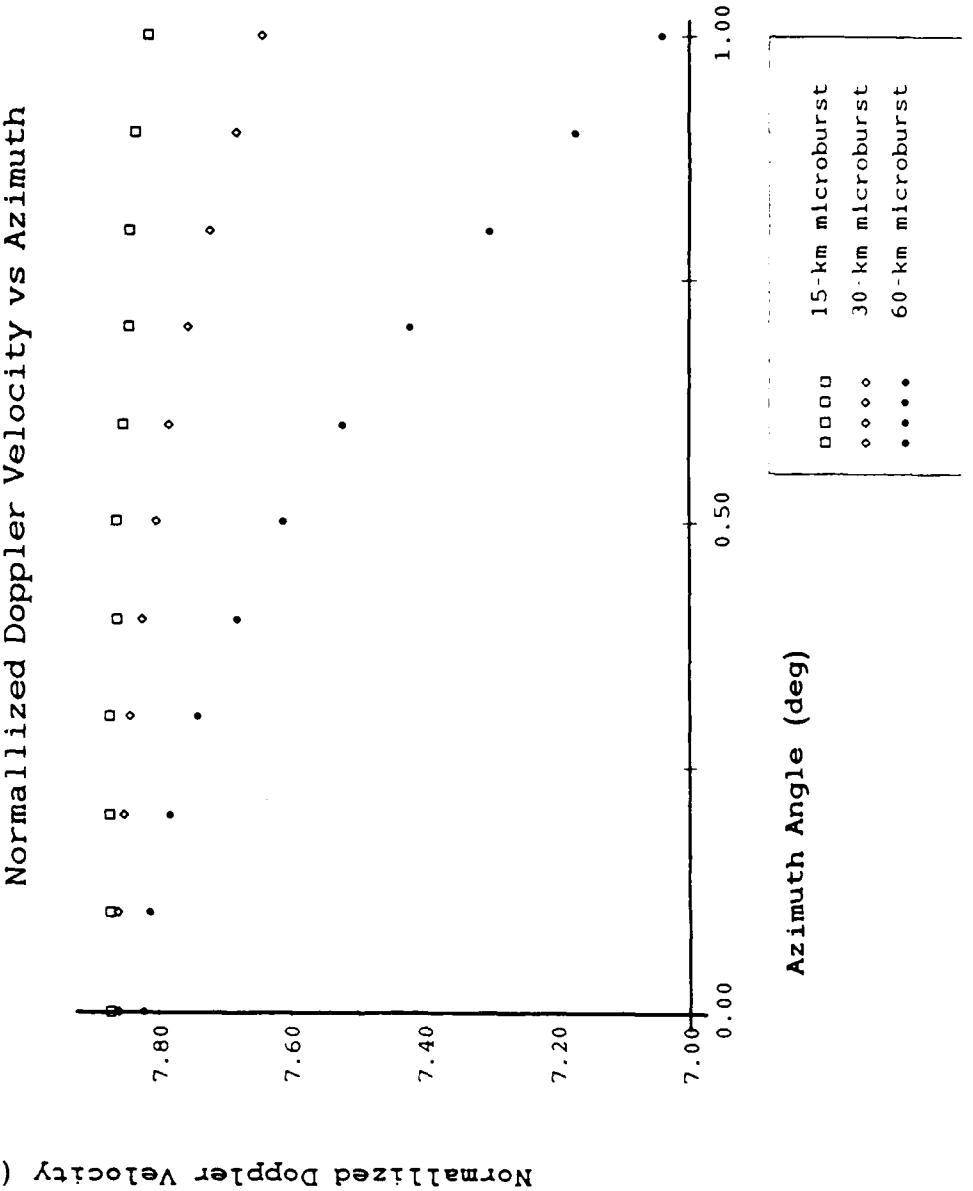

Figure 15. Radial shear normalized over range, plotted against azimuth angle, as in Fig. 13.

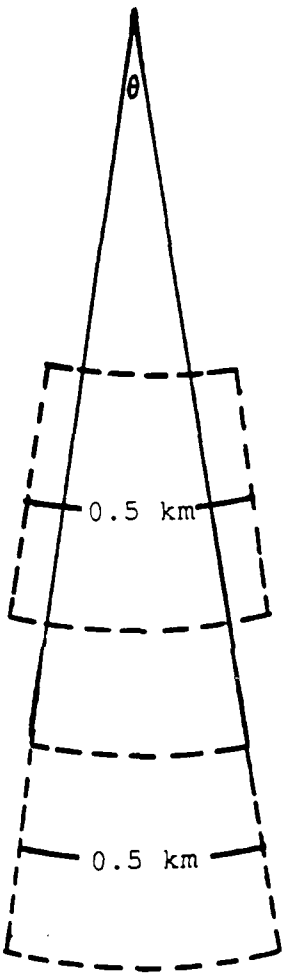

Figure 16. A schematic diagram describing the 0.5 km by 0.5 km grid used to further smooth the calculated Doppler velocities.

Figure 17. Smoothed Doppler velocities as a function of range and azimuth angle for a microburst centered 15 km from a single Doppler radar.

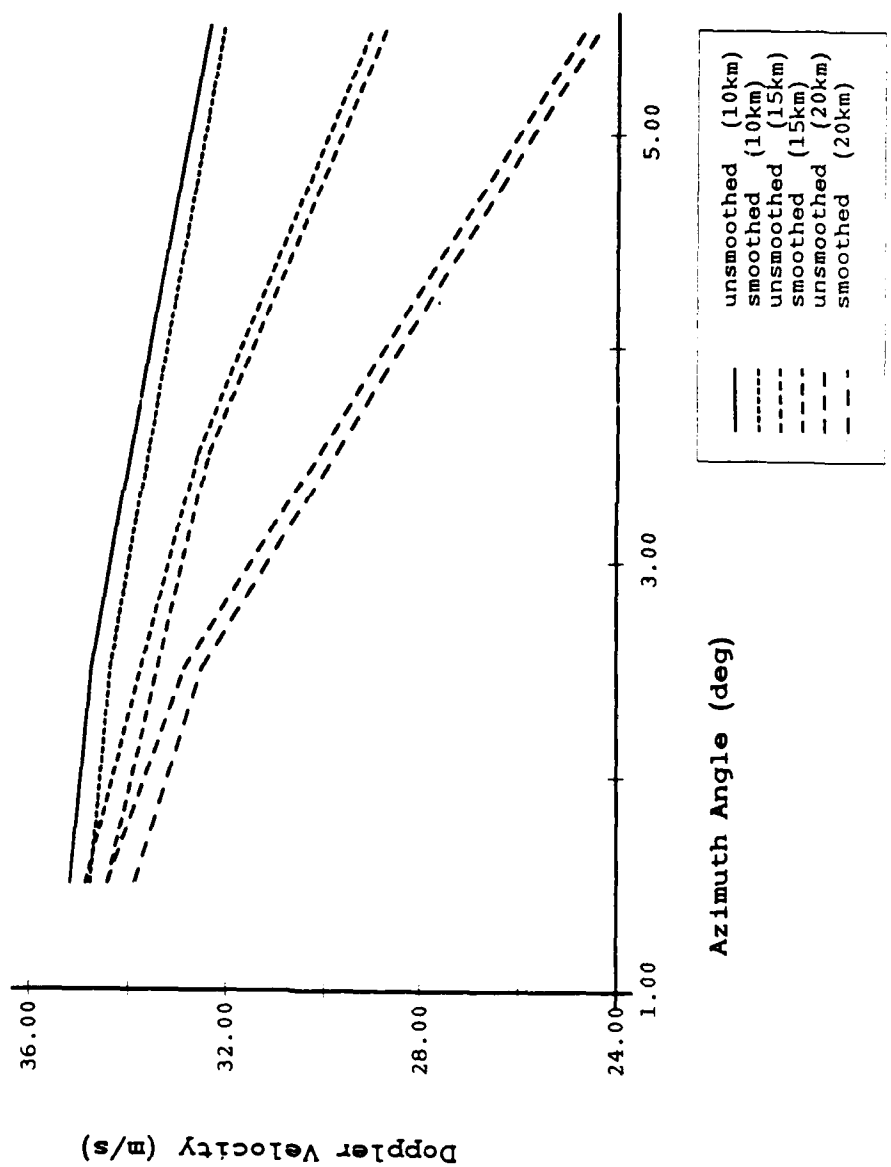

Figure 18. Doppler radial shear as a function of azimuth angle. Smoothed and unsmoothed velocities for microbursts centered at 10 km, 15 km, and 20 km from a single Doppler radar.

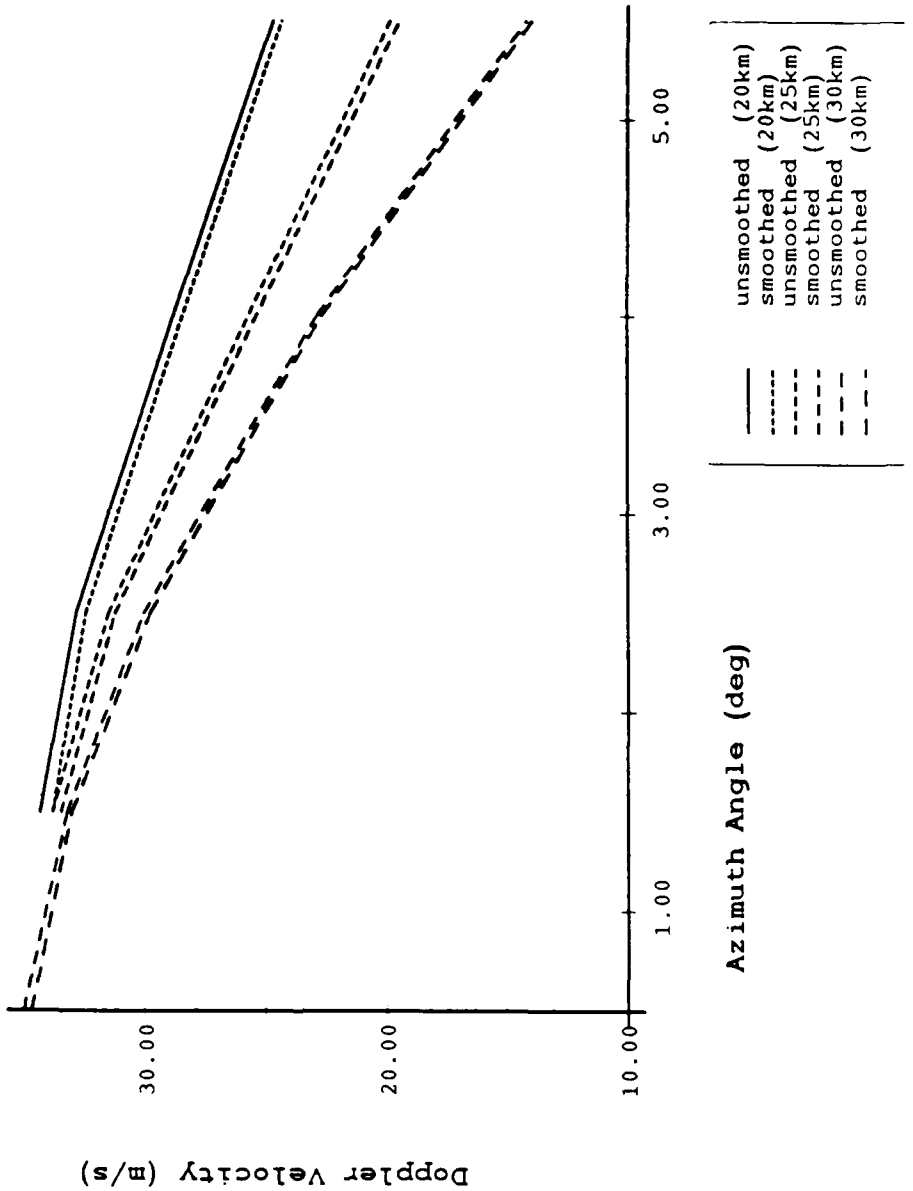

Figure 19. As in Fig.18, but for microbursts centered at 20 km, 25 km, and 30 km.

Figure 20. As in Fig.18, for azimuths between zero and one degree for a microburst centered at 15 km from a single Doppler radar.

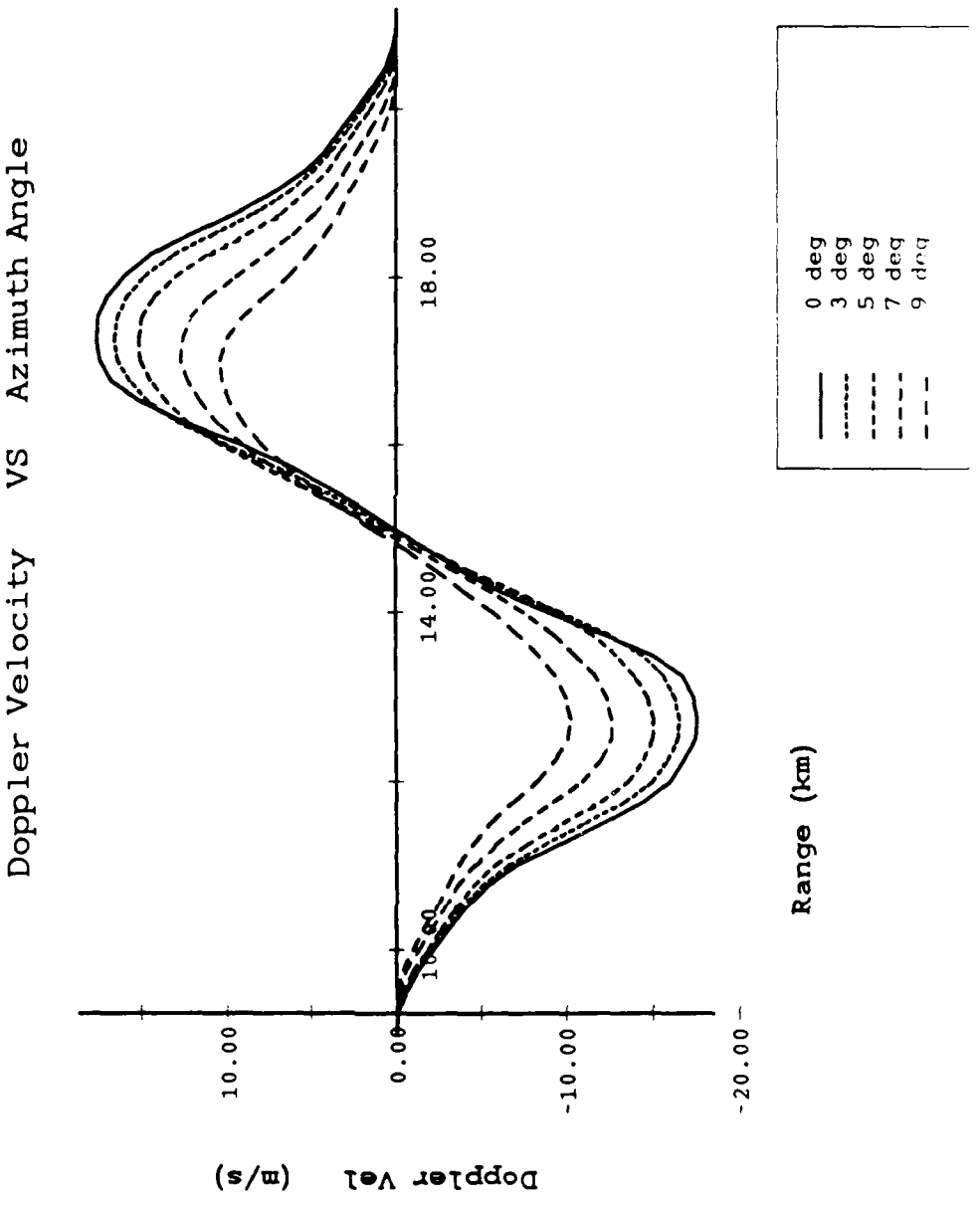

Figure 21. Doppler velocity as a function of range and azimuth angle for a microburst centered 15 km from a single Doppler radar.

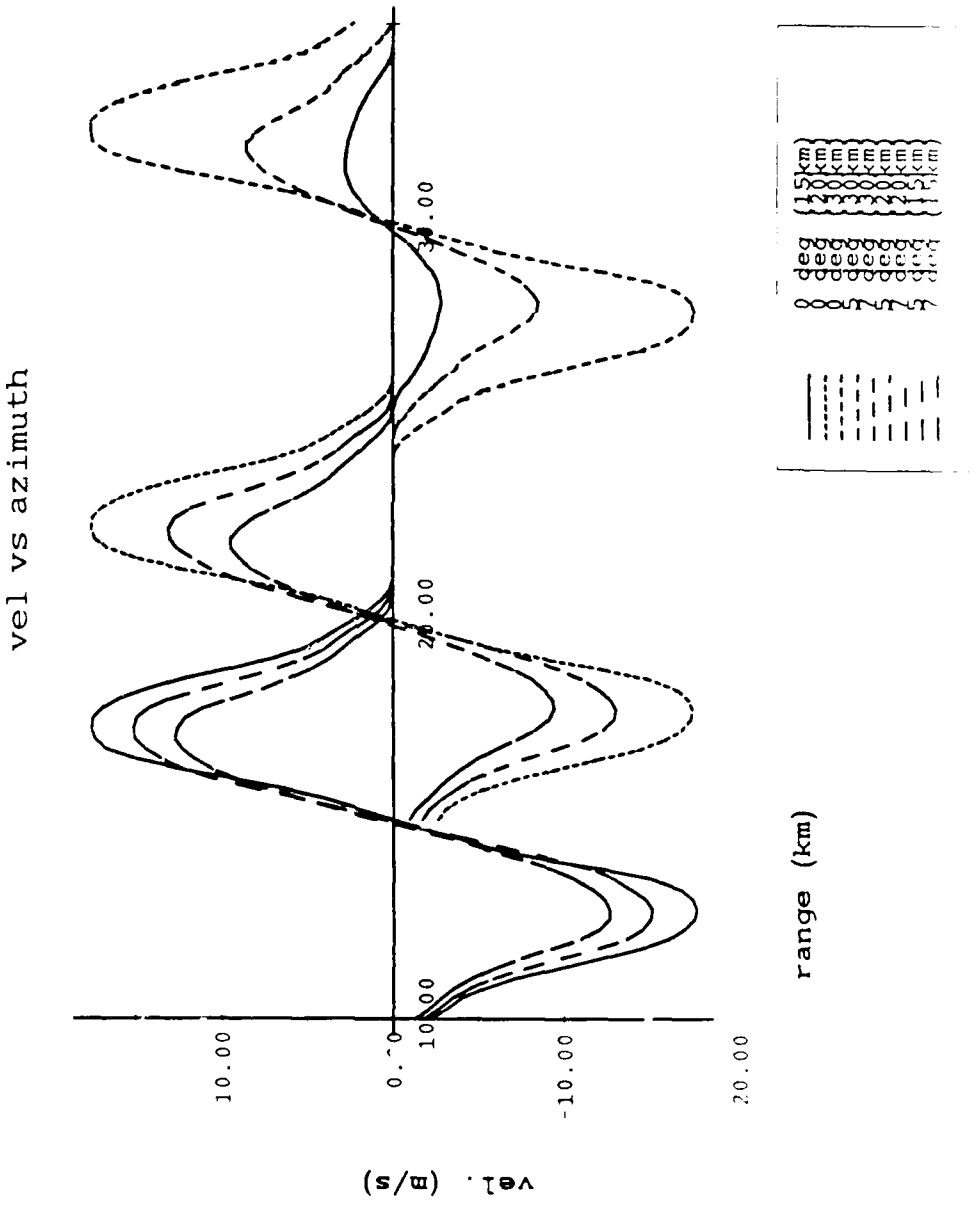

Figure 22. Doppler velocity as a function of range and azimuth angle for microbursts centered at 15 km, 20 km, and 30 km from a single Doppler radar.

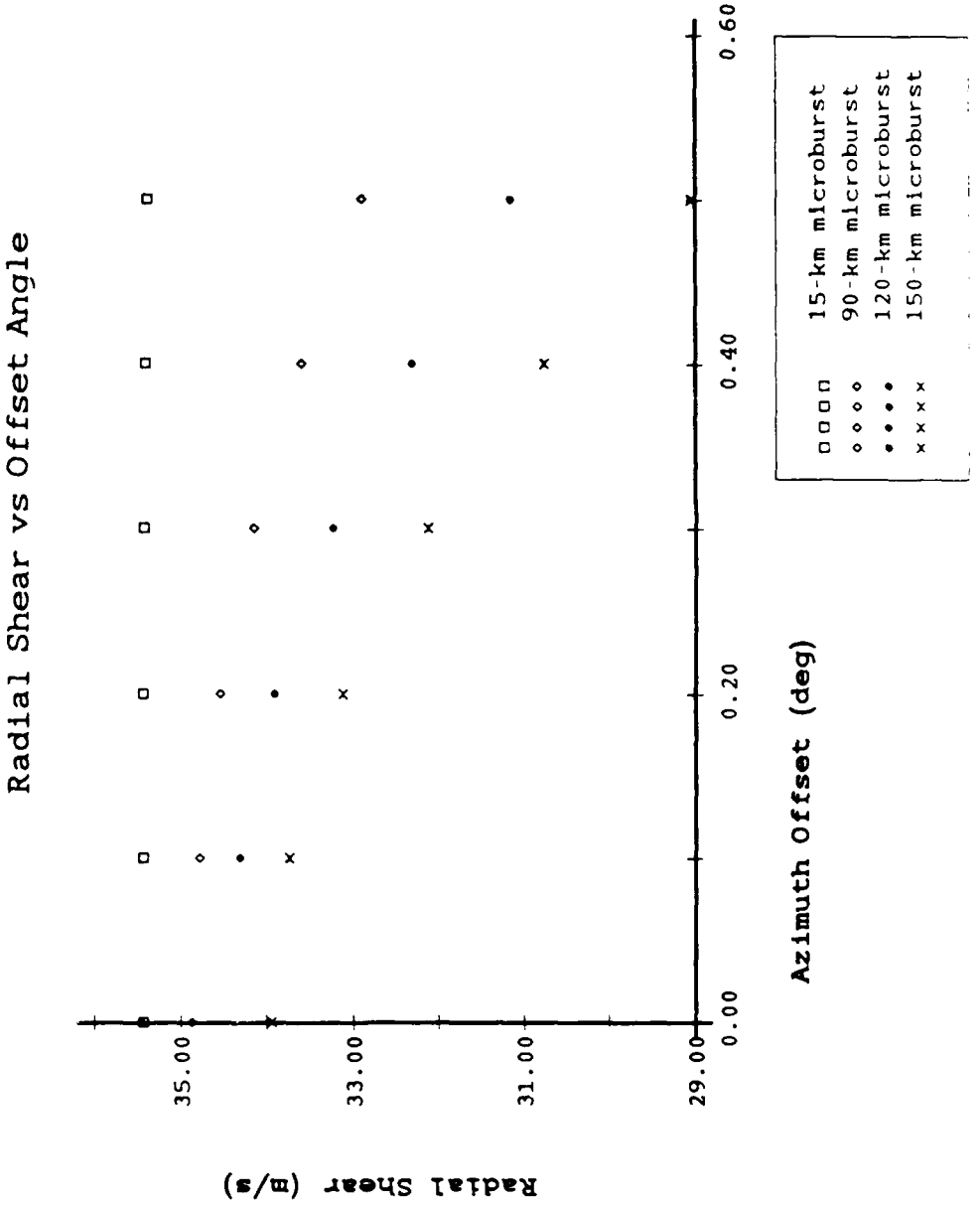

Figure 23. The radial shear plotted as a function of range and azimuth offset for microbursts centered 15 km, 90 km, 120 km and 150 km from a single Doppler radar.

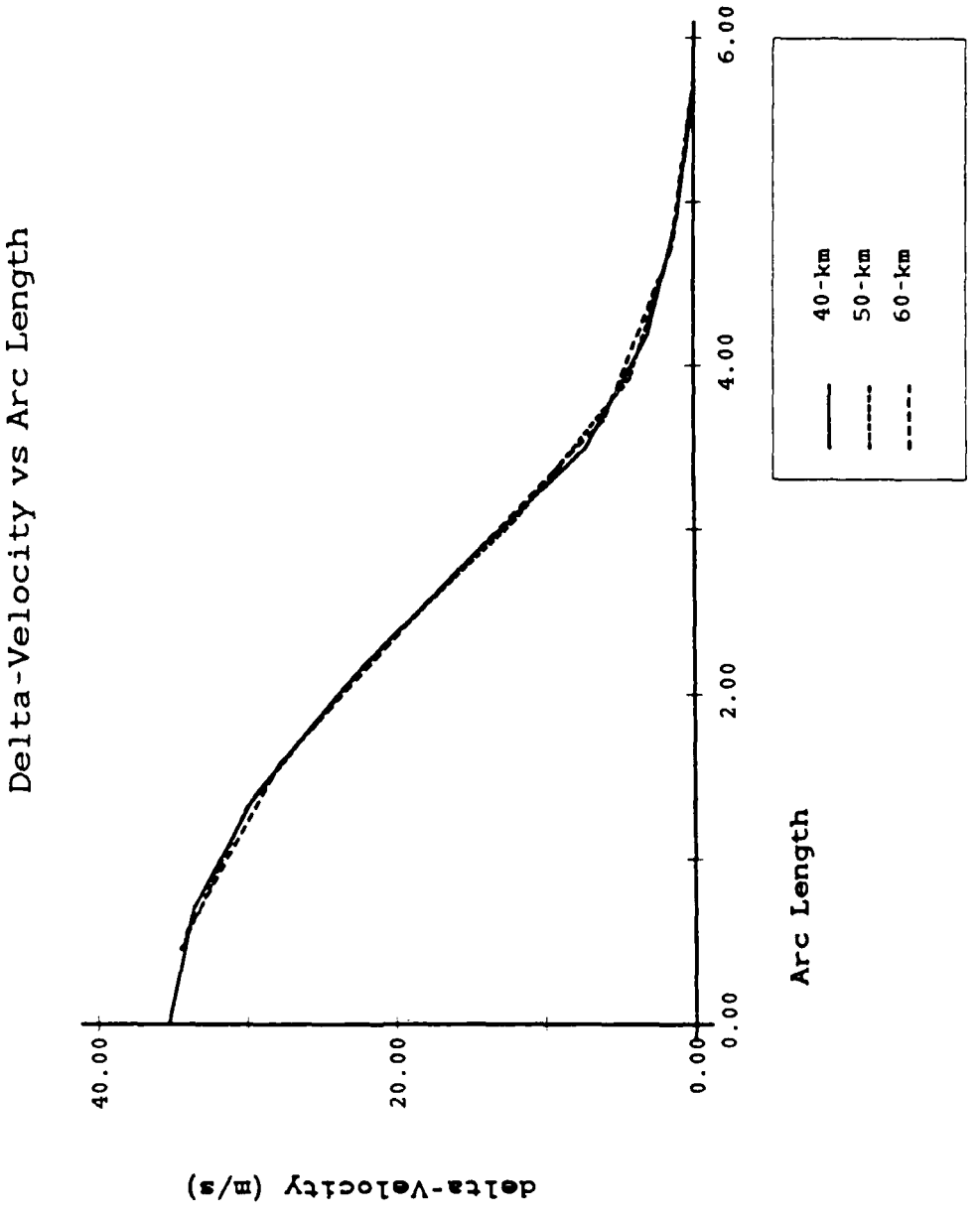

Figure 24. The radial shear plotted as a function of arc length for microbursts centered 30 km, 40 km, 50 km, and 60 km from a single Doppler radar.

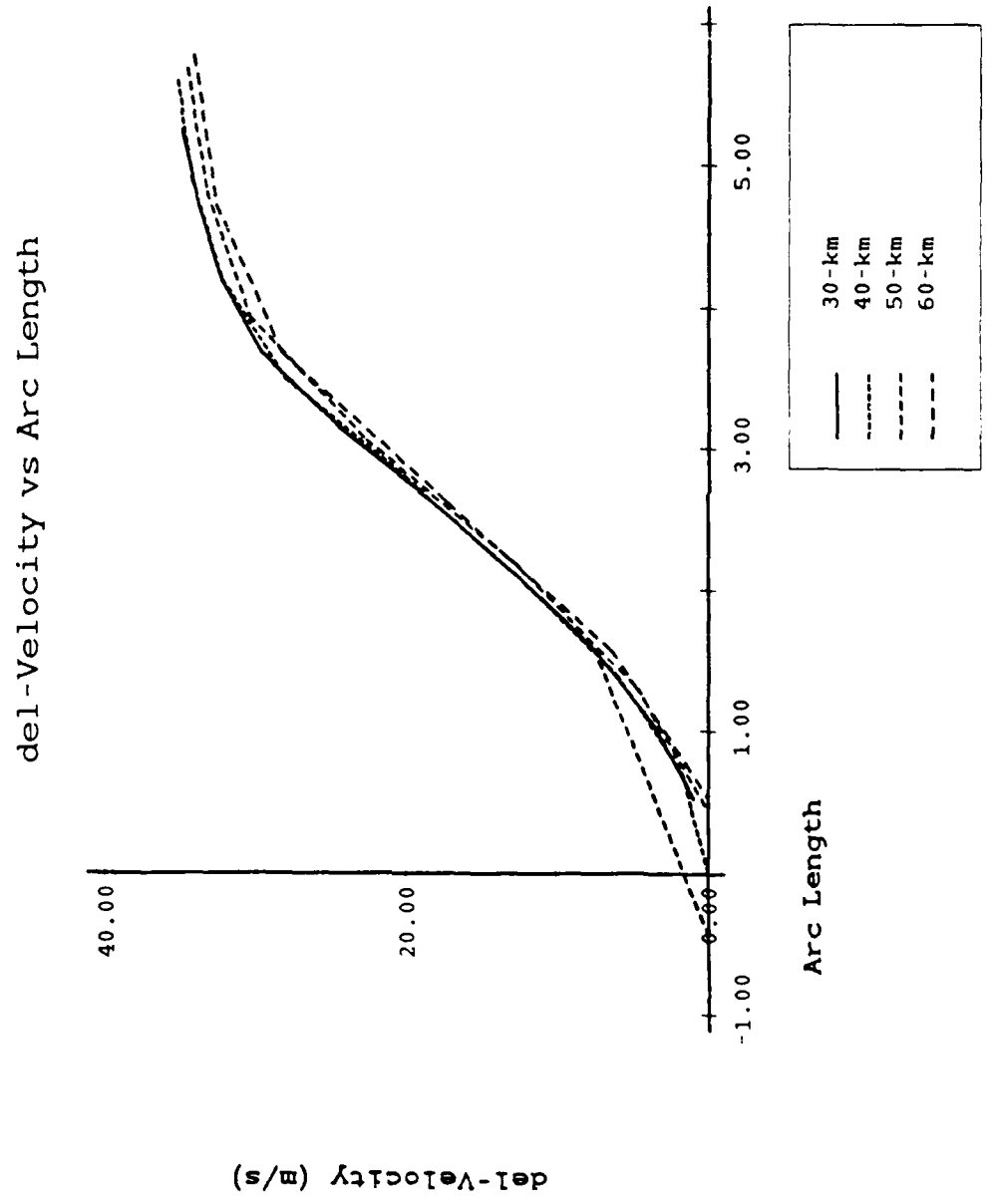

Figure 25. The maximum radial shear plotted as a function of arc length for microbursts centered 30 km, 40 km, 50 km, and 60 km from a single Doppler radar.

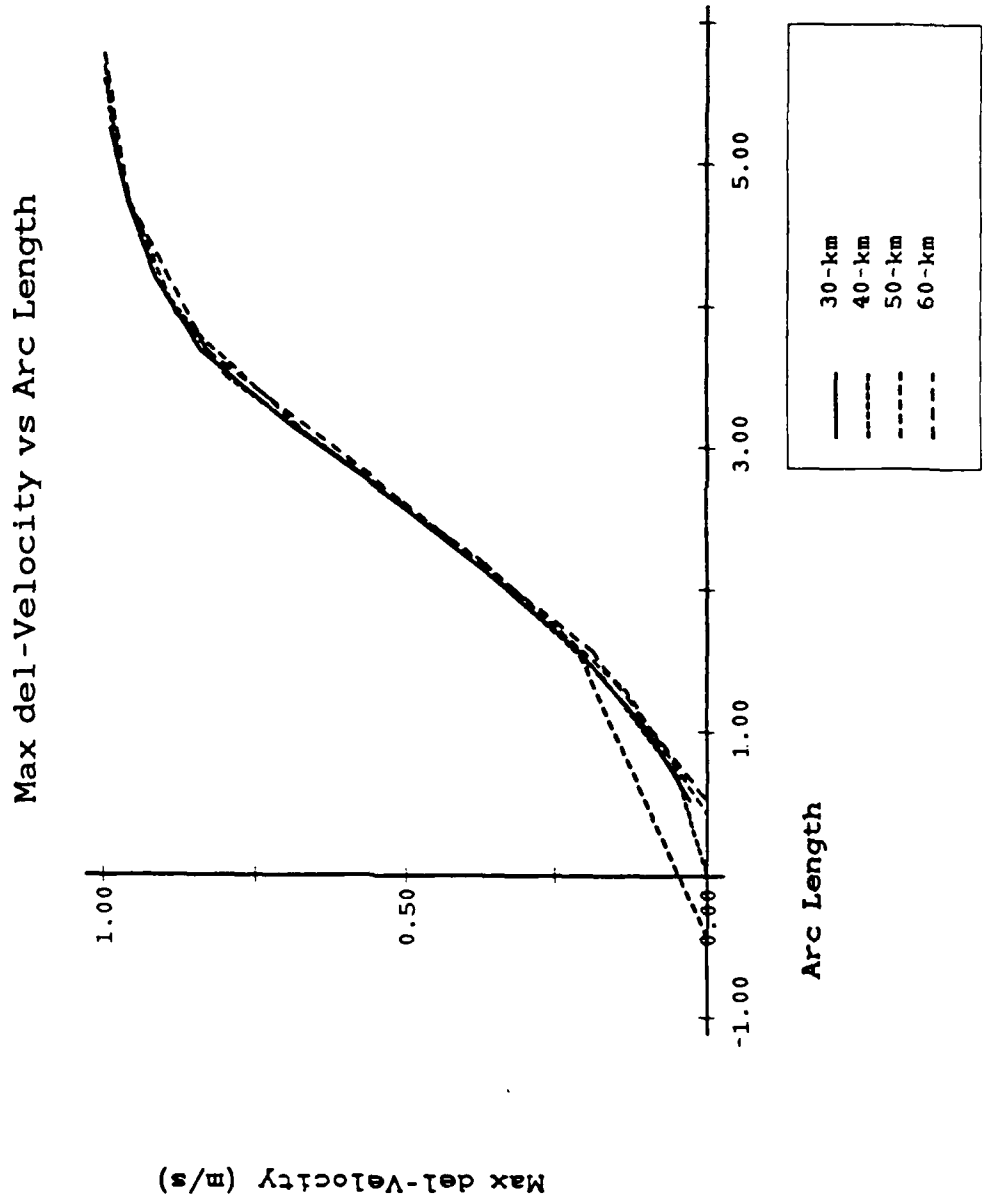

Figure 26. The maximum radial shear normalized by the radial shear for each azimuth angle plotted as a function of arc length for microbursts as in Fig. 24.

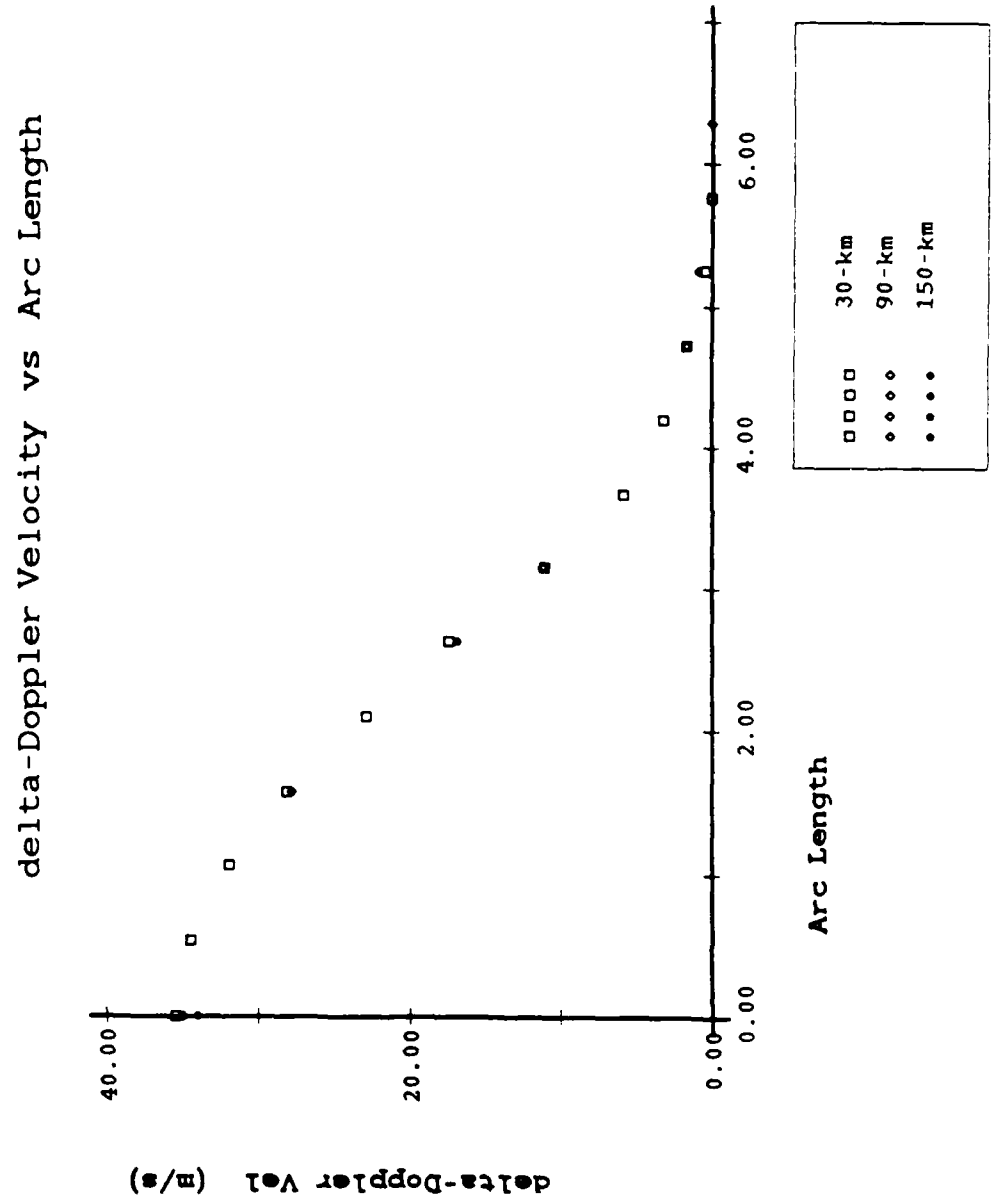

Figure 27. As in Fig. 24 but plotted as points, for microbursts centered 30 km, 90 km and 150 km from a single Doppler radar.

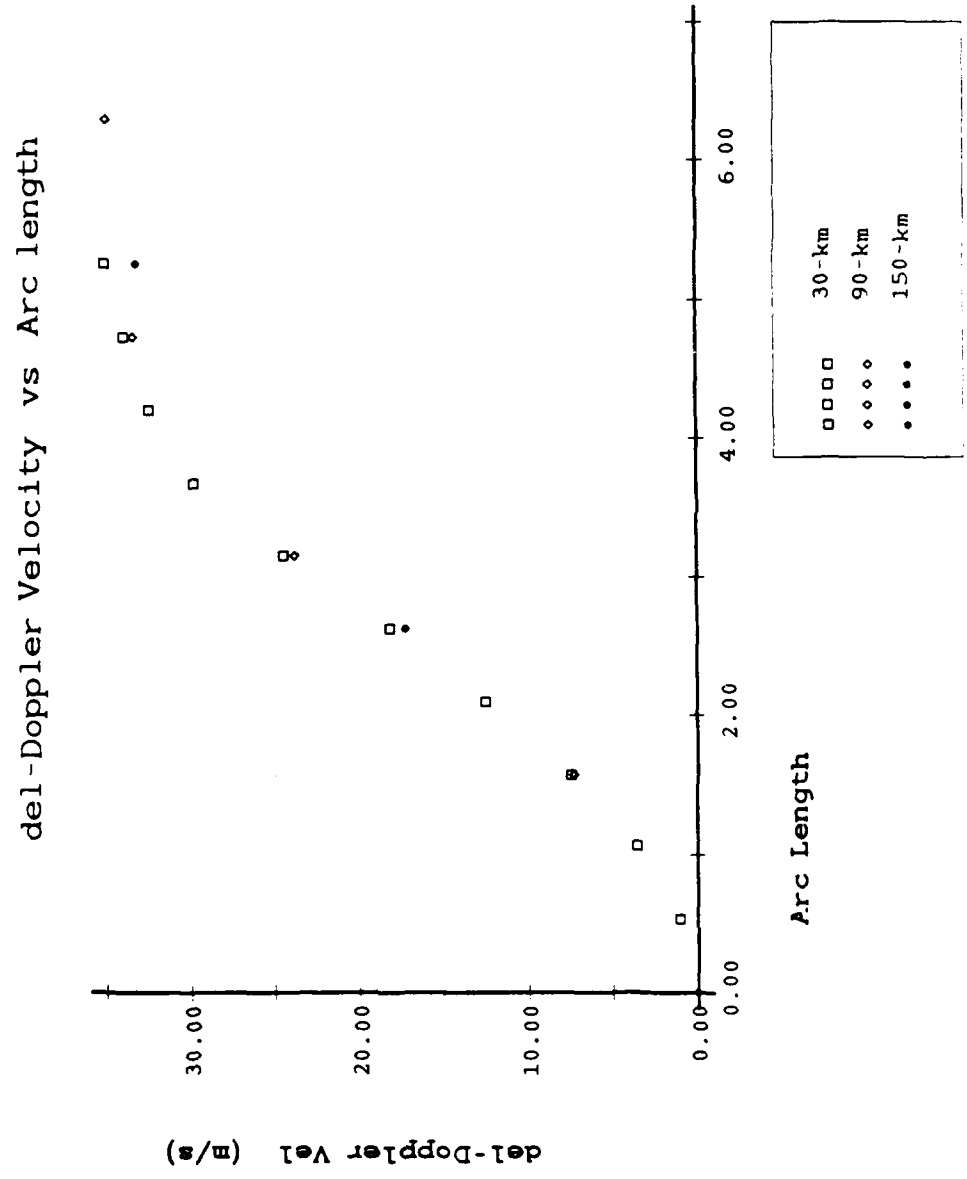

Figure 28. Parameters as in Fig. 25, but plotted as in Fig. 27.

Figure 29. Parameters as in Fig. 26, but plotted as in Fig. 27.

Figure 30. Parameters as in Fig. 24, for microbursts centered 30 km, 60 km, 90 km, 120 km, and 150 km from a single Doppler radar.

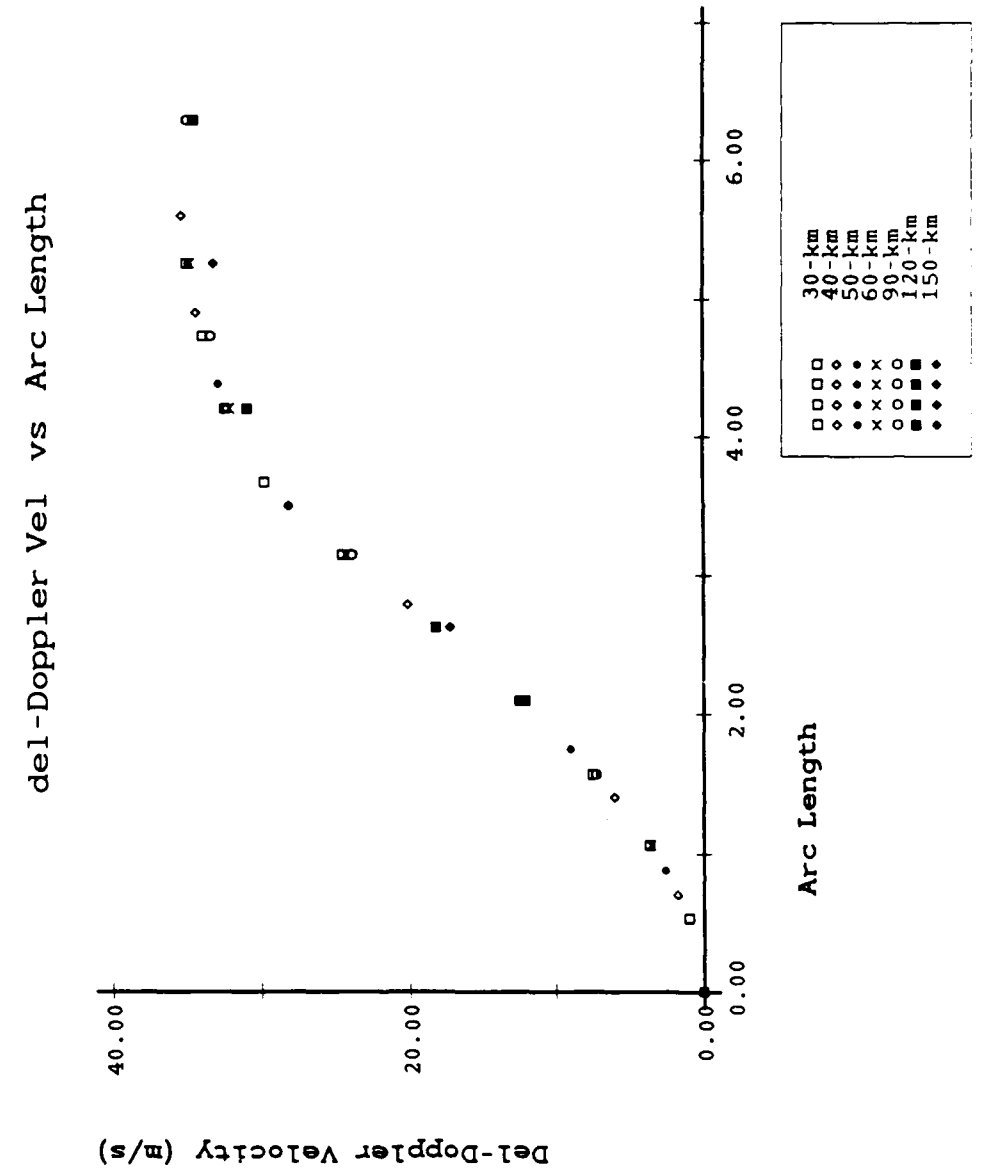

Figure 31. Parameters as in Fig. 25, but plotted as in Fig. 30.

Figure 32. Parameters as in Fig. 26, but plotted as in Fig. 30.

Table 1.
Gaussian-Squared Weighting Distribution Used to Smooth The Vertically-Averaged Doppler Velocities. Normalized weights are normalized by the sum of the weights. The azimuth angle is the offset from the center of the beam.

Azimuth	Weight	Normalized Weights
-0.4	0.25	0.0441
-0.3	0.46	0.0809
-0.2	0.71	0.1248
-0.1	0.92	0.1619
0.0	1.00	0.1766
0.1	0.92	0.1619
0.2	0.71	0.1248
0.3	0.46	0.0809
0.4	0.25	0.0441

Table 2.
Doppler Velocity Parameters as a Function of Azimuth Angle for Microbursts Centered 15 km and 30 km from a Single Doppler Radar. Azimuth angle is in degrees. Maximimum velocity away from the radar: Max +, maximum velocity towards the radar: Max (-). Radial shear is the difference between the two. Normalized velocity (Norm. Vel) is the velocity normalized over the difference in range between Max (+) and Max (-). All velocity-based parameters are in m/s. All velocity parameters determined from the vertically-averaged velocities (see Table 1).

Microburst centered at 15 km:

Azimuth	Max Vel (+)	Max Vel (-)	Radial Shear	Norm. Vel
0.00	17.712	17.711	35.423	7.87
1.00	17.584	17.582	35.166	7.81
3.00	16.636	16.645	33.281	7.40
5.00	14.990	15.030	30.021	6.67
7.00	12.781	12.773	25.554	6.01

Microburst centered at 30 km:

Azimuth	Max Vel (+)	Max Vel (-)	Radial Shear	Norm. Vel
0.00	17.686	17.686	35.372	7.86
1.00	17.193	17.192	34.385	7.64
3.00	13.964	13.956	27.920	6.20
5.00	8.648	8.617	17.265	4.60
7.00	2.860	2.871	5.731	1.64

Table 3.
Doppler Velocity Parameters as a Function of Azimuth Angle for a Microburst Centered Various Distances from a Single Doppler Radar. Azimuth angle is in degrees. Maximimum velocity away from the radar is Max (+), maximum velocity towards the radar is Max (-), radial shear is the difference between the two, normalized velocity (Norm. Vel) is the velocity normalized over the difference in range between Max (+) and Max (-); all are in m/s. All velocity parameters determined from the vertically averaged velocities (see Table 1).

Microburst centered at 15 km:

Azimuth	Max Vel (+)	Max Vel (-)	Radial Shear	Norm. Vel
0.00	17.712	17.711	35.423	7.87
0.10	17.710	17.710	35.420	7.87
0.20	17.706	17.706	35.413	7.87
0.30	17.700	17.700	35.400	7.87
0.40	17.691	17.690	35.381	7.86
0.50	17.680	17.679	35.358	7.86
0.60	17.665	17.664	35.330	7.85
0.70	17.649	17.647	35.296	7.84
0.80	17.630	17.628	35.258	7.84
0.90	17.608	17.606	35.214	7.83
1.00	17.584	17.582	35.166	7.81

Microburst centered at 30 km:

Azimuth	Max Vel (+)	Max Vel (-)	Radial Shear	Norm. Vel
0.00	17.686	17.686	35.372	7.86
0.10	17.681	17.681	35.362	7.86
0.20	17.666	17.665	35.331	7.85
0.30	17.640	17.640	35.280	7.84
0.40	17.605	17.604	35.209	7.82
0.50	17.560	17.558	35.118	7.80
0.60	17.505	17.503	35.008	7.78
0.70	17.440	17.439	34.879	7.75
0.80	17.367	17.365	34.731	7.72
0.90	17.284	17.282	34.567	7.68
1.00	17.193	17.192	34.385	7.64

Continued on the next page.

Table 3. - Continued.

Microburst centered at 60 km:

Azimuth	Max Vel (+)	Max Vel (-)	Radial Shear	Norm. Vel
0.00	17.587	17.586	35.173	7.82
0.10	17.567	17.566	35.133	7.81
0.20	17.509	17.508	35.017	7.78
0.30	17.412	17.412	34.824	7.74
0.40	17.280	17.280	34.560	7.68
0.50	17.113	17.114	34.227	7.61
0.60	16.914	16.915	33.829	7.52
0.70	16.684	16.686	33.370	7.42
0.80	16.425	16.429	32.854	7.30
0.90	16.139	16.145	32.284	7.17
1.00	15.828	15.835	31.663	7.04

Microburst centered at 90 km:

Azimuth	Max Vel (+)	Max Vel (-)	Radial Shear	Norm. Vel
0.00	17.428	17.428	34.856	7.75
0.10	17.387	17.387	34.774	7.73
0.20	17.265	17.265	34.530	7.67
0.30	17.064	17.064	34.128	7.58
0.40	16.788	16.790	33.578	7.46
0.50	16.444	16.446	32.890	7.31
0.60	16.032	16.035	32.067	7.13
0.70	15.559	15.560	31.119	6.92
0.80	15.026	15.026	30.052	6.68
0.90	14.442	14.438	28.880	6.42
1.00	13.806	13.800	27.606	6.13

Microburst centered at 120 km:

Azimuth	Max Vel (+)	Max Vel (-)	Radial Shear	Norm. Vel
0.00	17.221	17.220	34.441	7.65
0.10	17.149	17.150	34.299	7.62
0.20	16.945	16.946	33.891	7.53
0.30	16.610	16.610	33.220	7.38
0.40	16.151	16.150	32.301	7.18
0.50	15.572	15.574	31.146	6.92
0.60	14.886	14.887	29.773	6.62
0.70	14.098	14.093	28.191	6.26
0.80	13.220	13.200	26.420	5.87
0.90	12.250	12.213	24.463	5.44
1.00	11.189	11.167	22.356	5.26

Continued on next page

Table 3. - Continued.

Microburst centered at 150 km:

Azimuth	Max Vel (+)	Max Vel (-)	Radial Shear	Norm. Vel
0.00	16.964	16.963	33.927	7.54
0.10	16.862	16.864	33.726	7.49
0.20	16.554	16.556	33.110	7.36
0.30	16.055	16.055	32.110	7.14
0.40	15.376	15.373	30.749	6.83
0.50	14.520	14.515	29.035	6.45
0.60	13.496	13.482	26.978	6.00
0.70	12.321	12.292	24.613	5.47
0.80	11.040	11.026	22.066	5.19
0.90	9.733	9.723	19.456	4.86
1.00	8.410	8.385	16.795	4.20

Table 4.
Doppler Velocity Parameters as a Function of Arc Length for Microbursts Centered Various Distances from a Single Doppler Radar. ArcLngth is arc length in km. Radial shear is same as in Table 3, Difference is the difference between the radial shear and the max radial shear, both in m/s. Normalized velocity (Norm. Vel.) is the difference divided by the max radial shear and is dimensionless. All velocity parameters from the vertically-averaged velocities (see Table 1).

Microburst centered at 30 km and max radial shear 35.372:

ArcLngth	Radial Shear	Difference	Norm. Vel.
5.7596	0.010	35.362	0.9997
5.2360	0.462	34.910	0.9869
4.7124	1.551	33.821	0.9562
4.1888	3.082	32.290	0.9129
3.6652	5.731	29.641	0.8380
3.1416	10.997	24.375	0.6891
2.6180	17.265	18.107	0.5119
2.0944	22.868	12.504	0.3535
1.5708	27.920	7.452	0.2107
1.0472	31.787	3.585	0.1014
0.5236	34.385	0.987	0.0279
0.0000	35.372	0.000	0.0000

Microburst centered at 40 km and max radial shear 35.320:

ArcLngth	Radial Shear	Difference	Norm. Vel.
5.5851	0.081	35.239	0.9977
4.8869	1.121	34.199	0.9683
4.1888	3.084	32.236	0.9127
3.4907	7.234	28.086	0.7952
2.7925	15.217	20.103	0.5692
2.0944	22.853	12.467	0.3530
1.3963	29.316	6.004	0.1700
0.6981	33.633	1.687	0.0478
0.0000	35.320	0.000	0.0000

Continued on next page

Table 4. - Continued

Microburst centered at 50 km and max radial shear 35.253:

ArcLngth	Radial Shear	Difference	Norm. Vel.
5.6723	0.058	35.195	0.9984
4.7997	1.316	33.937	0.9627
3.9270	4.228	31.025	0.8801
3.4907	7.314	27.939	0.7925
2.6180	17.169	18.084	0.5130
2.1817	21.950	13.303	0.3774
1.3090	29.937	5.316	0.1508
0.4363	34.577	0.676	0.0192
0.0000	35.253	0.000	0.0000

Microburst centered at 60 km and max radial shear 34.227:

ArcLngth	Radial Shear	Difference	Norm. Vel.
5.7596	0.046	34.181	0.9987
4.1888	3.147	31.080	0.9081
3.6652	5.952	28.275	0.8261
3.1416	10.992	23.235	0.6789
2.6180	17.101	17.126	0.5004
2.0944	22.789	11.438	0.3342
1.5708	27.781	6.446	0.1883
1.0472	31.663	2.564	0.0749
0.5236	34.227	0.000	0.0000
0.0000	34.227	0.000	0.0000

Microburst centered at 90 km and max radial shear 34.856:

ArcLngth	Radial Shear	Difference	Norm. Vel.
6.2832	0.004	34.852	0.9999
4.7124	1.597	33.259	0.9542
3.1416	11.119	23.737	0.6810
1.5708	27.606	7.250	0.2080
1.0990	31.507	3.349	0.0961
0.6280	31.833	3.023	0.0867
0.3140	34.615	0.241	0.0069
0.0000	34.856	0.000	0.0000

Continued on next page

Table 4. - Continued

Microburst centered at 120 km and max radial shear 34.441:

ArcLngth	Radial Shear	Difference	Norm. Vel.
6.2832	0.023	34.418	0.9993
5.6549	0.257	34.184	0.9925
4.1888	3.609	30.832	0.8952
3.1416	11.315	23.126	0.6715
2.0944	22.356	12.085	0.3509
1.0472	31.147	3.294	0.0956
0.2094	34.299	0.142	0.0041
0.0000	34.441	0.000	0.0000

Microburst centered at 150 km and max radial shear 33.928:

ArcLngth	Radial Shear	Difference	Norm. Vel.
6.2832	0.063	33.865	0.9981
5.4978	0.512	33.416	0.9849
4.1888	3.994	29.934	0.8823
3.1416	11.549	22.379	0.6596
2.6180	16.975	16.953	0.4997
1.0472	30.749	3.179	0.0937
0.2618	33.725	0.203	0.0060
0.0000	33.928	0.000	0.0000

REFERENCES

Burrows, D.A. and L.F. Osborne, 1986: Precipitation loading in wet microbursts. Preprints, 23rd Conference on Radar Meteorology, Amer. Meteor. Soc., Boston, Ma., J97-J100.

Caracena, F. and M.W. Maier, 1987: Analysis of a microburst in the FACE meteorological mesonetwork in southern Florida. Mon. Wea. Rev., 115, 969-985.

Covey, D., 1983: Doppler weather radar principles. NOAA Training Paper NWS TC-1, 19 pp.

Eilts, M.D., 1986: Doppler radar measurement of low-altitude wind shear in Oklahoma. Preprints, 23rd Conference on Radar Meteorology, Amer. Meteor. Soc., Boston, Ma., J89- J92.

Elmore, K., 1986: Evolution of a microburst and bow-shaped echo during JAWS. Preprints, 23rd Conference on Radar Meteorology, Amer. Meteor. Soc., Boston, Ma., J101-J104.

Etkin, B., 1987: Comment on "A ring-vortex downburst model for flight simulation". J. Aircraft, 24, 479-480.

Fujita, T.T., 1983: Andrews AFB microburst. Six minutes after the touchdown of Air Force One. Pub. by Satellite and Mesometeorology Research Project (SMRP), Dept. of the Geophysical Sciences, The University of Chicago, SMRP Research Paper Number 205, 38 pp.

_____, 1985: The downburst. Pub. by Satellite and Mesometeorology Research Project (SMRP), Dept. of the Geophysical Sciences, The University of Chicago, SMRP Research Paper Number 210, 122 pp.

_____, 1986: DFW microburst. Pub. by Satellite and Mesometeorology Research Project (SMRP), Dept. of the Geophysical Sciences, The University of Chicago, SMRP Research Paper Number 21, 154 pp.

Hjelmfelt, M.R., 1984: Radar and surface data analysis of a microburst in JAWS. Preprints, 22nd Conference on Radar Meteorology, Amer. Meteor. Soc., Boston, Ma., 64-69.

_____ and R.D. Roberts, 1985: Microburst lines. Preprints, 14th Conference on Severe Local Storms, Amer. Meteor. Soc., Boston, Ma., 297-300.

Ivan, M., 1986: A ring-vortex downburst model for flight simulation. J. Aircraft, 23, 232-236.

Ivan, M., 1987: Reply by author by B. Etkin. J. Aircraft, 24, 480.

Jendrowski, P.J., 1986: Performance of quantitative parameters associated with the NEXRAD mesocyclone detection algorithm from simulated single doppler velocities. Master's Thesis, Dept. of Meteorology, The University of Maryland.

Kessinger, C.J., R.D. Roberts and K.L. Elmore, 1986: A summary of microburst characteristics from low-reflectivity storms. Preprints, 23rd Conference on Radar Meteorology, Amer. Meteor. Soc., Boston, Ma., J105-J108.

Leone, D.A., and G.E. Scott, 1984: NEXRAD site survey for Washington, D.C. (Sterling, Virginia site). Survey report 4 (draft). SRI Project 6273. Contract NA-83-SAC-00626. Prepared for The Department of Commerce, 70 pp.

McCarthy, J., R. Roberts, and W. Schreiber, 1983: JAWS data collection, analysis highlights and microburst statistics. Preprints, 21st Radar Meteorology Conference, Edmonton, Amer. Meteor. Soc., Boston, MA, 596-601.

_____, and J. Wilson, 1985: The Classify, Locate and Avoid Wind Shear (CLAWS) project at Denver's Stapleton International Airport: Operational testing of terminal weather hazard warnings with an emphasis on microburst wind shear. Preprints, 2nd International Conference on the Aviation Weather System, Amer. Meteor. Soc., 247-256.

_____, J.W. Wilson, and M.R. Hjelmfelt, 1986: Operational wind shear detection and warning: The "CLAWS" experience at Denver and future objectives. Preprints, 23rd Conference on Radar Meteorology, Amer. Meteor. Soc., Boston, Ma., R18-R21.

The NEXRAD Joint System Program Office (JSPO), 1986: Next generation weather radar product description document. Report No. R400-PD-202, 108 pp.

Rinehart, R.E. and M.A. Isaminger, 1986: Radar characteristics of microbursts in the mid South. Preprints, 23rd Conference on Radar Meteorology, Amer. Meteor. Soc., Boston, Ma., J116-J119.

Roberts, R.D. and J.W. Wilson, 1984: Precipitation and kinematic structure of microburst producing storms. Preprints, 22nd Conference on Radar Meteorology, Amer. Meteor. Soc., Boston, Ma., 71-76.

_____ and _____, 1986: Nowcasting microburst events using single Doppler radar data. Preprints, 23rd Conference on Radar Meteorology, Amer. Meteor. Soc., Boston, Ma., R14-R17.

Wilk, K. E., 1985: Weather services in the '90s, Proceedings. Published by the MITRE Corporation.

Wilson, J.W., C. Kessinger, R.D. Roberts, and J. McCarthy, 1984: Microburst wind structure and evaluation of Doppler radar for wind shear detection. Final Report. DOT/FAA/PM-84/29, 29 pp.

Zhu, S. and B. Etkin, 1985: Model of the wind field in a downburst. J. Aircraft, 22, 595-601.